WAVE PROPAGATION IN ANISOTROPIC ROCKS

Semiannual Technical Report No. 1

Contract No. H02[illegible]0021

Sponsored by Advanced Research Projects Agency, ARPA Order No. 1579, Amend. 3

Program Code 62701D

Principal Investigator: Dr. W. Goldsmith
Faculty Investigator: Dr. J. L. Sackman

University of California
Berkeley, California 94720

Sept. 25, 1972

DOCUMENT CONTROL DATA - R & D

(Security classification of title, body of abstract and indexing annotation must be entered when the overall report is classified)

1. ORIGINATING ACTIVITY (Corporate author) University of California, Berkeley	2a. REPORT SECURITY CLASSIFICATION Unclassified 2b. GROUP

3. REPORT TITLE

WAVE PROPAGATION IN ANISOTROPIC ROCKS, III

4. DESCRIPTIVE NOTES (Type of report and inclusive dates)

Semiannual Technical Report, February 23, 1972 to August 31, 1972

5. AUTHOR(S) (First name, middle initial, last name)

Werner Goldsmith and Jerome L. Sackman

6. REPORT DATE September 30, 1972	7a. TOTAL NO. OF PAGES 92	7b. NO. OF REFS 6
8a. CONTRACT OR GRANT NO. HO220021 b. PROJECT NO c. ARPA Order No. 1579, Amend. 3 d. Program Code No. 62701D	9a. ORIGINATOR'S REPORT NUMBER(S) 3 9b. OTHER REPORT NO(S) (Any other numbers that may be assigned this report)	

10. DISTRIBUTION STATEMENT

Distribution of this document is unlimited

11. SUPPLEMENTARY NOTES	12. SPONSORING MILITARY ACTIVITY Advanced Research Projects Agency

13. ABSTRACT

This report summarizes progress on the analytical and experimental aspects of the investigation concerned with wave propagation resulting from impact on a Yule marble block and an investigation of its mechanical properties. The system was modeled as a transversely isotropic halfspace with the elastic symmetry axis lying in the free surface, loaded by a concentrated normal force of arbitrary time variation. The analysis for the displacements, strains and stresses in the interior is complete and numerical results have been obtained by integral transform methods. A corresponding finite element program has also been completed. Transducer packages for the measurement of stresses in the interior of a Yule marble block have been developed, calibrated and tested. Drilling and embedment techniques for the testing of the Yule marble blocks under actual impact conditions have been evolved. Static and dynamic tests in tension and compression for various orientations of samples have been completed as well as cyclic loading, creep and some fracture tests.

DD FORM 1 NOV 65 1473 (PAGE 1)

S/N 0101-807-6801

14 KEY WORDS	LINK A		LINK B		LINK C	
	ROLE	WT	ROLE	WT	ROLE	WT
Rock mechanics						
Properties of rock						
Fracture of rock						
Wave propagation						
Anisotrpic Half-spaces						
Impact						
Transient signals in rocks						
Transducers						
Finite element analysis						
Integral transform techniques						

ib

SEMIANNUAL TECHNICAL REPORT NUMBER ONE

ARPA Order Number: 1579, Amendment 3

Program Code Number: 62701D

Contractor: The Regents of the University of California

Effective Date of Contract: February 23, 1972

Contract Expiration Date: February 22, 1973

Amount of Contract: $62,436.00

Contract Number: H0220021

Principal Investigator: Professor W. Goldsmith, (415)642-3739

Project Engineer: Professor J. L. Sackman (415)642-2950

Title: "Wave Propagation in Anisotropic Rocks"

Report Period: February 23, 1972 to August 31, 1972

Sponsored by

Advanced Research Projects Agency

ARPA Order No. 1579 Amend. 3

Program Code 62701D

This research was supported by the Advanced Research Projects Agency of the Department of Defense and was monitored by the Bureau of Mines under Contract No. H0220021.

SEMIANNUAL TECHNICAL REPORT NUMBER ONE

ARPA Order Number: 1579, Amendment 3

Program Code Number: 62701D

Contractor: The Regents of the University of California

Effective Date of Contract: February 23, 1972

Contract Expiration Date: February 22, 1973

Amount of Contract: $62,436.00

Contract Number: H0220021

Principal Investigator: Professor W. Goldsmith, (415)642-3739

Project Engineer: Professor J. L. Sackman (415)642-2950

Title: "Wave Propagation in Anisotropic Rocks"

Report Period: February 23, 1972 to August 31, 1972

Sponsored by

Advanced Research Projects Agency

ARPA Order No. 1579 Amend. 3

Program Code 62701D

This research was supported by the Advanced Research Projects Agency of the Department of Defense and was monitored by the Bureau of Mines under Contract No. H0220021.

SUMMARY

This report summarizes progress on the analytical and experimental aspects of the investigation concerned with wave propagation resulting from impact on a Yule marble block and an investigation of its mechanical properties. The system was modeled as a transversely isotropic halfspace with the elastic symmetry axis lying in the free surface, loaded by a concentrated normal force of arbitrary time variation. The analysis for the displacements, strains and stresses in the interior is complete and numerical results have been obtained by integral transform methods. A corresponding finite element program has also been completed. Transducer packages for the measurement of stresses in the interior of a Yule marble block have been developed, calibrated and tested. Drilling and embedment techniques for the testing of the Yule marble blocks under actual impact conditions have been evolved. Static and dynamic tests in tension and compression for various orientations of samples have been completed as well as cyclic loading, creep and some fracture tests.

INTRODUCTION

This report represents the first semi-annual technical report under contract H0220021 between the U. S. Bureau of Mines and the University of California on the subject entitled "Wave Propagation in Anisotropic Rocks." The current contract period from February 23, 1972 to February 22, 1973 represents the second year of the program; the present document summarizes progress up to August 31, 1972, with emphasis on the work completed since the beginning of the second year of the contract. A full account of the activities on this project during the first year of its existence may be found in Reference 1.*

The scope of the program is detailed in the proposal identified as UCB-Eng 3286 dated April 26, 1971 and submitted on behalf of the University of California, Berkeley, by W. Goldsmith as Principal Investigator and is also spelled out in Artile I of the subject contract. A program schedule was also submitted at the end of March, 1972; this schedule has been faithfully observed with the exception of the work on fracture initiation and propagation; in some areas, however, the work is progressing ahead of schedule.

The work has been subdivided into the following categories:

(a) Theoretical Examination of the Wave Propagation in an Anisotropic Solid.

(b) Experimental Examination of Wave Propagation in an Anisotropic Solid.

*Bibliography appears at the end of the text.

(c) Experimental Determination of the Physical Properties of Yule Marble under Static and Dynamic Loading.

The following personnel have been employed on the project during the report period: (a) Mr. S. L. Suh who is concerned with the development and evaluation of the history of the field variables in a transversely isotropic half-space subject to an impact on its free surface using integral transform methods, (b) Mr. M. Katona who completed the first phase in the development of a finite-element program for the solution of the subject problem and who has since departed to resume his permanent position with the U. S. Navy, (c) Mr. R. Kenner who assisted in various tasks as a Fortran programmer, but departed for an industrial position in April, (d) Mr. G. Dasgupta who has taken over the completion of the subsequent phases of the finite element analysis, (e) Mr. K. Krishnamoorthy who has been concerned with category (b) of the investigation, (f) Mr. Tom Jones who has been assisting Mr. Krishnamoorthy in the development of experimental equipment, (g) Mr. S. Howe who has been assigned to the pursuit of category (c), assisted for a brief period by Mr. J. Thorington, and two laboratory assistants, Mr. E. Lin and Mr. G. Wilcox. Messrs. Suh , Katona, Dasgupta, Krishnamoorthy and Howe will use or have used part or all of their work under this contract as part or all of their graduate research requirements. Supervision and active collaboration have been provided by Professors W. Goldsmith and J. L. Sackman who are responsible for the conduct of the program. In the development of the finite element program, the expert assistance of Prof. R. L. Taylor of the Department of Civil Engineering, University of California,

Berkeley without compensation is gratefully acknowledged.

The only technical difficulty that has been encountered during the first six months of the present contract that is as yet unresolved concerns the evaluation of the surface displacements of a transversely isotropic half-space under the action of a concentrated, time-dependent surface load. This quantity cannot be obtained directly from the corresponding solution of the interior displacements evaluated at the free surface, but rather must be analyzed as an independent problem. It appears that the crux of the difficulty may lie in the accuracy of the numerical evaluation of the integration that converts the two-dimensional solutions to the three-dimensional situation. This phase of the investigation will be further scrutinized during the remainder of the contract period.

Another difficulty concerns appropriate staffing of the investigation. Although it was anticipated that the portion of the program dealing with fracture iniatiation and propagation could not be completed during the first two years of the contract, it was hoped to make a significant start in this direction by securing the services of a graduate student, Mr. J. Thorington, who expressed considerable interest in pursuing research in the area of fracture of brittle materials. However, after a very brief association with the project, Mr. Thorington accepted a full-time position in industry for financial reasons. Consequently, a replacement must be located and suitably trained which will considerably delay the planned execution of this phase of the project.

The remainder of the report will be concerned with a more detailed technical description of the progress achieved.

2. SUMMARY OF PROGRESS ACHIEVED DURING FIRST YEAR OF INVESTIGATION

The integral transform technique was developed and partially tested to obtain the displacement field in the transversely isotropic solid with an axis located in the free surface under a Heaviside input. This process constructed a three-dimensional solution from the integration of a series of two-dimensional problems associated with line loads on the surface of the half-space. It employed a Cagniard-de Hoope transformation which simplified the inversion process and led to a physical interpretation of the transient wave process in terms of well-established concepts of wave and slowness surfaces that have been employed in the field of crystal acoustics.

A finite element program had been written for the three-dimensional problem cited above and was in the debugging and test phase. It had also been specialized to the simpler case of isotropic behavior where other solutions for checking purposes exist. Results obtained at that time included the uniaxial wave process in a rod and the surface motion of a half-space.

In the experimental wave propagation phase, the major accomplishments achieved at that time included the development of a crystal transducer package with a laterally unconstrained crystal employed as a sensing element, the calibration of both the crystal and the entire package, the development of installation techniques for the embedment of the transducer inside cores drilled in rock bars, and some progress

in the development of a suitable grouting material to fill the core holea after inatallation of the tranaducer unit with a minimum of dynamic miamatch.

Crystallographic techniquea were developed for the location of the axia of elastic aymmetry of the Yule marble apecimens. Static compreaaive testa, aome with repeated loading, were conducted on samplea of the material, indicating aignificant non-linearities and the preaence of hystereais. A technique was developed for the generation of constant atrain ratea in the intermediate range of 10 to 100 aec^{-1} utilizing an adaptation of a Hopkinson-bar procedure.

3. PROGRESS DURING REPORTING PERIOD

(a) Theoretical Examination of Wave Proceasea

(1) Integral Tranaform Approach

Introduction

It was reported previoualy [1] that alownesa, velocity, and wave curvea for the Yule marble characterized by the elastic conatanta obtained by Ricketts [2], have been evaluated. Furthermore, Cagniard-de Hoope paths for different angular ranges of the medium were generated. From these, diaplacement fielda in the half-apace due to a point load representing a Heaviaide function of time denoted as the fundamental diaplacement aolution, were conatructed. Corresponding computer programs were written to perform the required numerical evaluationa. During the laat aix montha, formulations for the displacements, atrains and streaaes produced by a realiatic input have been obtained by uae of convolution integrala in conjunction with the

fundamental solutions. Also, a computer program for the above with an sssumed realistic force input given by $I = I_o \sin^2\left(\frac{\pi t}{t^*}\right)$ has been written and corresponding curves for several positions in the medium have been obtained.

During the next six months, it is planned to check the solution and to compare numerical results both with experimental data, yet to be obtained, and with the results of a corresponding finite element analysis. An additional effort will be extended to obtain numerical results on the surface of the half-space. Some exploratory efforts may also be directed towards obtsining numerical results for the displacement fields due to a point source in the medium and possibly for an orthotropic material

Formulations

i) Body Waves

As indicated in Eq. (35) of Ref. [1], the diaplacement response in a transversely isotropic half-space subjected to a force normal to the free surface represented by a Heaviside time function may be expressed as

$$u_{k_H}(\vec{x},t) = -\frac{1}{2\pi^2 \rho R} \int_{-\frac{\pi}{2}}^{\frac{\pi}{2}} d\theta \left[\sum_{j=1}^{3} \mathrm{Re}\left[W_k^j (t,\rho,\theta,\tilde{\theta},Q,R) \right] P_j \frac{\partial P_j}{\partial t} H(t-t_j) \right]$$

$$(k = 1,2,3) \qquad (1)$$

in which $p_{(i)} = p_{(i)}(t,R,\theta,\tilde{\theta},Q)$ is a Cagniard-de Hoop path defined by Eqs. (29) and (30) of Ref. [1].

θ is an angle defined in the slowness space,

t is the time,

$\vec{x}$ is the position vector of a response point in a Cartesian coordinate system in the medium

$(R, \tilde{\theta}, Q)$ is the position of a response point in spherical coordinates,

$W_k^{(j)}$ are complex algebraic functions

$H(t) = \begin{matrix} 1 \text{ if } t > 0 \\ 0 \text{ if } t < 0 \end{matrix}$ is the Heaviside function, and

Re[ ] indicates the real part of a complex quantity.

In Eq. (1), k represents the component of the displacement field in a Cartesian system, and j indicates the numbering of the roots of Eqs. (29) and (30) of Ref. [1].

Equation (1) was utilized to obtain displacements resulting from the input of an arbitrary time function through a convolution integral. Let $I = I(t)$ be the time history of the surface force, then the corresponding displacement $u_k(\vec{x},t)$ is given by

$$u_k(\vec{x},t) = \int_0^t \dot{I}(t-t') \, u_{k_H}(\vec{x},t') \, dt' \qquad (2)$$

where

$$\dot{I}(t) = \frac{dI(t)}{dt} ,$$

and t' is a dummy variable.

The displacement gradients which will be used to compute strain fields are obtained analytically by simply taking spatial derivatives of Eq. (2). In the usual indicial notation,

$$u_{k,j}(\vec{x},t) = \frac{\partial u_k(\vec{x},t)}{\partial x_j} = \int_0^t \dot{I}(t-t') \frac{\partial u_{k_H}}{\partial x_j}(\vec{x},t')\, dt' \qquad (3)$$

Though Eq. (3) appears simple, the expression is actually quite involved because u_{k_H} are complicated implicit functions of x_j as can be seen by inspection of Eq. (1). For the purpose of writing and testing a computer program which carries out the convolution integral indicated by Eq. (2), the input force has been taken in the form

$$I(t) = I_0 \sin^2\left(\frac{\pi t}{t^*}\right) \qquad (4)$$

where I_0 is the amplitude, and t^* is the duration of the input pulse. It turns out that expression (4) is a good approximation for the input force produced when a steel ball is dropped vertically onto the free surface of a half-space. The time derivative of Eq. (4) is

$$\dot{I}(t) = \frac{I_0 \pi}{t^*} \sin\left(\frac{2\pi t}{t^*}\right) \qquad (5)$$

which is to be substituted into Eq. (3). It is convenient to introduce a parameter $\tau = \frac{t}{R}$, where R is the distance from the impact point on the free surface of the half-space to a receiver in the medium. Rewriting Eq. (3) by use of Eq. (5) results in the following

$$u_k(\vec{x},t) = -\frac{I_0}{2\pi\rho t^*} \int_0^\tau \sin 2\pi\left(\frac{\tau-\tau'}{\tau^*}\right) u_{k_H}(\vec{x},\tau')\, d\tau' \qquad (6)$$

where $\tau^* = \frac{t^*}{R}$. This represents the displacement field under the input force given by Eq. (4). From the infinitesimal theory of elasticity, the components of the strain tensor are defined as

$$e_{ij} = \frac{1}{2}\,(u_{i,j} + u_{j,i}) \qquad (i,j = 1,2,3) \tag{7}$$

where $u_{i,j}$ are given by Eq. (3), and the components of the stress tensor are expressed as

$$\sigma_{ij} = c_{ijk\ell}\, e_{k\ell} \qquad (i,j,k,\ell = 1,2,3) \tag{8}$$

For a transversely isotropic medium, $c_{ijk\ell}$ consists of 5 independent constants. These were obtained experimentally by Ricketts [2] for the Yule marble considered here.

It is convenient to use a reduced form of Eq. (8) written as

$$\sigma_I = c_{IJ}\, e_J \qquad (I,J = 1,2,3,\ldots,6) \tag{8}$$

where $\sigma_1 = \sigma_{11}$, $\sigma_2 = \sigma_{22}$,..., $e_1 = e_{11}$, $e_2 = e_{22}$,..., and $c_{11} = c_{1111}$, $c_{12} = c_{1122}$,... etc. [2]. The matrix form of Eq. (8) for the computer programming may be expressed as

$$\begin{pmatrix} \sigma_1 \\ \sigma_2 \\ \sigma_3 \\ \sigma_4 \\ \sigma_5 \\ \sigma_6 \end{pmatrix} = \begin{pmatrix} c_{11} & c_{12} & c_{13} & 0 & 0 & 0 \\ c_{12} & c_{11} & c_{13} & 0 & 0 & 0 \\ c_{13} & c_{13} & c_{33} & 0 & 0 & 0 \\ 0 & 0 & 0 & c_{44} & 0 & 0 \\ 0 & 0 & 0 & 0 & c_{44} & 0 \\ 0 & 0 & 00 & 0 & \frac{1}{2} & (c_{11}-c_{12}) \end{pmatrix} \begin{pmatrix} e_1 \\ e_2 \\ e_3 \\ e_4 \\ e_5 \\ e_6 \end{pmatrix} \tag{9}$$

In the existing computer program which evaluated fundamental displacement solutions given by (1), a subroutine which performs a convolution integration simultaneously for the three Cartesian components of displacement has been incorporated, debugged and tested using the input force given by Eq. (4). Furthermore, a subroutine which finds displacement gradients given by Eq. (3), strains given by Eq. (7), and stresses given by Eq. (8)′ has been written and tested. A listing of this program will be included in the final report.

ii) Surface Motion

For the surface motion, the Cagniard-deHoop paths defined by Eqs. (29) and (30) of Ref. [1] collapse into the real axis on the p-plane on which the Cagniard-deHoop paths are defined [1]. However, a simple pole lies on the real axis which corresponds to the Rayleigh pole for the isotropic medium. The presence of the simple pole at $p = -\frac{1}{v_R}$, where v_R is the phase velocity of the Rayleigh wave, requires an indentation of the path of integration to avoid the pole. When this is done, the points on a small semicircular indentation

around the pole no longer corresponds to real time. Therefore, the contribution from the pole was obtained separately from those of ordinary points on the Cagniard-deHoop path and expressed as

$$u_{k_{H\,pole}}(x_1,0,x_3,t) = B_1\, H\left(t - \frac{r}{v_R(\tilde{\theta},\theta)}\right) \tag{10}$$

The Heaviside function appears in the relation above instead of the Dirac-delta function $\delta\left(t - \frac{r}{v_R(\tilde{\theta},\theta)}\right)$ which was incorrectly exhibited in Eq. (36) of Ref. [1]. To obtain solutions for a realistic input for the displacements, strains and stresses, a procedure analogous to that employed for the body wave solution may be applied.

Results and Discussions

1) Body Waves

A subroutine which finds the roots of the Cagniard-deHoop path by solving a quartic algebraic equation has been modified so as to be faster and more accurate. This is rather important since most of the computing time is spent in finding the roots of the quartic equation defining the path. Examples of the output obtained from the computer program for the force input given by Eq. (4) will be presented. Three components of the fundamental displacement u_1, u_2 and u_3 along a ray at $\tilde{\theta} = 80°$, $\varphi = 45°$, which lies in the fan of critical angular ranges for both $\tilde{\theta}$ and φ, [1], are shown in Fig. 1. As can be seen, although the u_2 component appears very much like the Heaviside function in time, u_1 and u_3 exhibit a sharp change in shape at

$\tau\left(\frac{1}{R}\right) \cong 1.0 \times 10^{-5}$ which is approximately the arrival time for the quasi-shear waves. All three components of the displacement approach their static values at approximately $\tau \simeq 2 \times 10^{-5}$. Curves along other rays have also been obtained, although they are not included here. The ratios of the amplitudes of the three components become quite different depending on the angles $\tilde{\theta}$ and φ. Figures 2, 3, 4 and 5 represent convolved components of displacement of Eq. (6) for the same ray as shown in Fig. 1 but with R = 1,2,5,10 inches, respectively. As can be seen from this sequence, the amplitudes of the displacements decrease proportionately to $\frac{1}{R}$ as would be expected for the body wave.

In the evaluation of the convolution integral of Eq.(6), the time steps employed were, $\Delta\tau = 1 \times 10^{-6}$, 2.08×10^{-6}, 8.33×10^{-7}, and 4.1×10^{-7} for Figs. 2,3,4 and 5 respectively. It can be seen that the $\Delta\tau$ employed for Fig. 3 appears to have been too big resulting in curves which are distorted compared to the other results obtained with smaller integration steps. Figures 6,7,8,9 and 10 represent the fundamental normal strain components e_{11}, e_{22}, e_{33}, the convolved strain components e_{11}, e_{22}, e_{33}, e_{12}, e_{13} and e_{23} for the input force given by Eq. (4), the fundamental normal stress components σ_{11}, σ_{22}, σ_{33} and the convolved normal stresses σ_{11}, σ_{22} and σ_{33}, respectively, along a ray defined by $\tilde{\theta} = 80°$, $\varphi = 45°$. As can be seen, the fundamental strains as well as the fundamental stresses vary rapidly for the range of τ which lies between 6×10^{-6} and 1.5×10^{-5} and they appear to approach their static values at a time of about $\tau = 2 \times 10^{-5}$. The above time interval brackets the

arrival times of the two quasi-shear waves for this medium.

Additional stress and strain data have been obtained, but are not included in the present report. The total time to compute the fundamental as well as the convolved displacements, strains and stresses was about 7 seconds on the CDC 7600 computer for a single receiver point.

ii) Surface Motion

The Rayleigh function for this medium has been checked against Buchwald's expression [3] who utilized a plane wave approach. A program giving the Rayleigh wave speeds for different directions on the free surface of the half-space has been developed. A program which computes fundamental displacements on the surface from a Heaviside input force has also been written. The results obtained show spurious oscillatory motion for the time intervals from zero to the time of the Rayleigh wave arrival, although, at later times the solution appears to be reasonable. The cause of this difficulty has not yet been determined. For this reason, no further attempt to compute convolved quantities has been made at this moment but effort will be directed toward resolving this problem during the next 6 months.

iii) A computer program which plots the history of a field variable at a given receiver point has been written using the GDS-CALCOM system [4] developed at the Computer Center of the University of California, Berkeley. This program was used to produce the plots presented here.

Conclusions

A program which yields displacements, strains and stresses for an input of the form of Eq. (4) has been developed. This program computes above quantities in the half-space except on the free surface and on the vertical axis given by $\varphi = 90^{\circ}$. These numerical results will be checked against experimental data and results derived from a finite element program. The program which computes surface displacements will be examined and possible modifications will be attempted to correct suspected arrors. If time is available an attempt will be made to modify the program so as to solve the similar boundary value problem for an orthotropic material. Finally a solution to the problem of an internal source in the half-space may be examined.

2. FINITE ELEMENT METHOD

The annual report [1] contains in detail the formulation of the algorithm used in the finite element method of solution of wave propagation problems. Mr. M. Katona authored a report [5] that is presently employed as a user's guide. This report described the solution algorithm and contained a discussion of the stability of the explicit method of solution and the choice of integration time step. Mr. Katona enlarged the Finite Element Assembly Program (FEAP) originally written by Professor Robert L. Taylor of the Department of Civil Engineering, University of California, Berkeley, adding two main subroutines, namely EXPLCT (for explicit time integration) and DYNPLT (to give printer plots of stress evolution). An option was provided to input any desired pulse shape either as a prescribed function or as a table of values of the impulsive force at each time

step.

Reference [5] described the results of some wave propagation problems used to check the accuracy and efficiency of the coding developed. The case of a column subjected to a triangular load impulse was run, modelling the system with a stack of three dimensional elements with eight nodes per element (the so-called "Brick-8 element") and with Poisson's ratio $\nu = 0$. It was observed in the numerical solution that a nondispersive stress pulse propagated down the column as predicted by the analytical solution for the one-dimensional wave propagation problem. Encouraging numerical results were also obtained upon comparing the surface displacement for wave propagation in an isotropic half space modelled by axisymmetric elements with the theoretical solution. A problem involving a sine-squared impulse acting on the surface of an anisotropic half space using the three dimensional general anisotropic element was also evaluated. A study of the time steps in the solution indicated that the latter is practically insensitive to their size provided they are smaller than the critical one.

The report also includes a discussion of an efficient way of modelling half space problems with a finite number of elements. In this procedure, the maximum dilatational wave speed in the medium was estimated as the bar speed with the largest constitutive modulus. From the largest coordinate in the region of interest and from the duration of the pulse the total solution time of interest is estimated at that station so as to include the effect of the entire input pulse. Then the size of the finite element model is evaluated such that no

reflections could arrive from the finite boundary at the point of interest during the solution period. With an assumed mesh density (normally 8 to 10 per pulse length), the element size for adequate discretization was obtained. Calculations for the time step used in the explicit integration scheme for the desired time span and for blank common storage required to execute the FEAP coding are also contained in Ref. [5].

Examples of input data for various problems were given and an updated version of the user's manual was included. The input instructions were also given on the use of the general isotropic solid element, the axisymmetric, isotropic solid element and the general anisotropic solid element.

Professor R. L. Taylor introduced many changes in the program after March 1972, and made the program more efficient. He introduced a section to estimate the critical time step. For a step larger than the estimated one, the program gives an error message and stops execution. This is to prevent the user from encountering numerical instabilities due to the time of transmission of a disturbance through an element being less than the integration time step. Without modifying the algorithm some statements in the EXPLCT subroutine were changed to increase the computing speed by about ten percent.

Cases were run for the problem of wave propagation through an isotropic rock block both with a sine-squared impulse and an experimentally-measured load history. Good correspondence with the experimental results was observed as far as the radial stress σ_{rr} is

concerned; however, the axial stress σ_{zz} did not compare to a satisfactory degree. This indicates that the FEAP program should be reexamined to check the accuracy of the numerical analysis; in addition, the experimental calibration procedure should be further verified.

At present the following modifications in the program are being considered; a) the output option in the entire program is to be changed radically so as to obtain only those outputs of interest. Thus, for the four point quadrilateral element, only the center stress will be printed out as the others at the corners are of no significant value. (b) The present time step estimate for the stability check is very conservative as the eigenvalue is calculated at the element level. A section will be added to calculate the largest eigenvalue of the full stiffness matrix. This may add to the economy of running as it might be possible to use a larger time step than presently.

It is intended to prepare and publish a report containing all the details of the FEAP program, with a listing and with elaborate user's instructions in the next six months.

(b) Experimental Examination of the Wave Processes in an Anisotropic Rock Material

The examination of body and surface waves will be conducted using the two available blocks of Yule marble whose dimensions are 24" x 24" x 10" . In order to attain this objective a program of experimental work was completed during the first year of the contract to develop the necessary body-wave sensors and the technique of

embedding the sensors in the Yule marble blocks. The first annual report [1] contains a description of the initial experimental efforts to achieve this goal. The present report is a continuation of this earlier work. The main accomplishment to be reported at the present stage of the overall research project is the completion of the development work leading to the suitable design, adequate calibration methods and successful embedding technique of the body-wave sensors. Actual measurements have been made using these body-wave sensors embedded in a block of limestone which is nearly isotropic. A method of loading the free surface by means of sphere impacts through an intermediate loading bar has been used for these measurements which was found to be convenient because it permitted repeatability of the test, allowed measurement of the input pulse, and permitted close control of the impact conditions. The monitoring of the loading pulse by means of an input crystal at the contact point has also been successfully accomplished. In the sequel further details will be given.

As reported in [1], at the end of the first year of contract, a number of experiments were conducted establishing the design of crystal transducers which could be suitably calibrated. Further experiments indicated that these crystal transducers could be installed in deep holes, leads extracted out and the remaining voids filled with a suitable grouting material. A mixture of alumina and epoxy in appropriate proportions was considered as a possible filler material. However, since a metal bar with a crystal transducer

mounted at one end could be inserted with ease into a deep hole, the previously developed quartz crystal transducer was redesigned as shown in Fig. 11. Since magnesium has an acoustic impedance closely matching the average acoustic impedance of Yule marble, such a transducer package was constructed using a 3/16" diameter rod of magnesium. A block of sandstone 14" x 12" x 9" was obtained and one face of it was machined flat. A 3/16" diameter hole was core drilled in the center of the block from the bottom. The transducer package was inserted in the hole. Smearing the bar with wax before insertion enabled the bar to be held firmly in the block with the crystal transducer anchored securely at about 1½" from the free surface. Simple drop tests with 1/2" diameter steel balls indicated that the quartz crystal was not sensitive enough. Also, a reexamination of the piezoelectric relations of x-cut quartz crystals showed that even though x-cut quartz crystals are suitable for one dimensional experiments, because of the coupling between the piezoelectric constants of x-cut quartz crystals, they are not suitable for obtaining the truly unidirectional stress in a complex stress field. Thus a transition from x-cut quartz crystals to the more sensitive PZT-5a crystals was made. In these ceramic crystals the absence of coupling between the piezoelastic constants enables the measurement of a truly unidirectional stress even in a complex stress field. However, the lateral surface of the crystal must still remain free as in the case of x-cut quartz. Table 1 shows the comparison of the appropriate piezoelectric relations and constants for x-cut quartz and PZT-5a crystals.

PIEZOELECTRIC MATERIAL	NONZERO PIEZOELECTRIC CONSTANTS & RELATIONS [6]	PIEZOELECTRIC CONSTANT FOR COMPRESSION MODE			ACTUAL DIMENSIONS OF CRYSTALS USED	SUPPLIER OF CRYSTALS	WHERE USED IN THE PROJECT
		DESIGNATION	PUBLISHED VALUE $\frac{pc/in^2}{Lb/in^2}$	EXPERIMENTAL VALUE $\frac{pc/in^2}{Lb/in^2}$			
Quartz	$d_{11}, d_{12}, d_{14}, d_{25}, d_{26}$ $d_{12} = -d_{11}$, $d_{25} = -d_{14}$ and $d_{26} = 2d_{11}$	d_{11}	10.01 [5]	10.2 [1]	1/8" Dia.X 0.031" Thick	X-Tron Electronics, Inc. Hayward, California	Rock bars [1]
Ceramic PZT-5a	$d_{33}, d_{31}, d_{32}, d_{15}, d_{24}$	d_{33}	1650 [6]	1557 [Present Report]	1/8" Dia.X 0.031" Thick	Valpey-Fischer Corp. Holliston, Mass.	Limestone block [Present report]
Ceramic PZT-4	$d_{31} = d_{32}$, $d_{15} = d_{24}$	d_{33}	1232 [6]	Not yet established.	1/16"Dia.X 0.020" Thick	International Transducer Corp., Goleta, California.	To be used in Yule marble blocks.

TABLE 1: COMPARISON OF PIEZOELECTRIC CONSTANTS OF QUARTZ AND PZT CERAMIC CRYSTALS.

The choice of magnesium as a suitable material for the transducer package was governed by the close match in the acoustic impedance of magnesium and the average acoustic impedance of Yule marble material. A comparison of the physical properties of Yule marble and the various materials used in the PZT-5a crystal transducer package is presented in Table 2.

The PZT-5a ceramic crystals, 1/8" dia. x 1/32" thick were obtained from Valpey Fischer Corporation, Massachusetts. A transducer package was constructed as shown in Fig. 11 with the PZT-5a crystal replacing the quartz crystal. Again the bar was smeared with wax and the package was inserted in the sandstone block to within $1\frac{1}{2}$" from the free surface. Simple drop tests by 1/4" diameter steel spheres showed that the crystals were extremely sensitive. The experimental arrangement is shown in Fig. 12. Typical records obtained by two different sphere impacts directly above the crystal package are shown in Figs. 13 and 14. In Fig. 13 the record was obtained by voltage amplification and in Fig. 14 charge amplification was used [1]. The shapes of the pulses and the degree of sensitivity indicated that pulses could be recorded deep in a block of rock material. However, the crystals and the transducer packages had to be calibrated before any quantitative results could be established.

The calibration of x-cut quartz crystals was made using an aluminum split Hopkinson bar technique. But magnesium and PZT-5a crystals were found to be not compatible in the sense that they do not have the same acoustic impedance in the relevant direction of the crystals. However, since the discontinuity is small compared to the pulse length, magnesium split Hopkinson bar was used to test the

crystals. Thus a number of quality control tests were made using a 1/8" diameter split Hopkinson bar of magnesium. The experimental arrangement is shown in Fig. 15. Since the PZT-5a crystals were highly sensitive, a 100x attenuator was used before the output was recorded on the oscilloscope. The crystal output was compared with the strain gage output. In view of the rather high crystal outputs interfering with the strain gage circuit, as shown in Fig. 16 by the drastic deviation in the output from the strain gage station upon initiation of the crystal signal, which has a peak value of 400V to 500V, the output from the strain gage station immediately after the crystal station was not recorded. However, a comparison of the strain gage response and the attenuated crystal response for a number of crystals indicated that the crystals were essentially identical. In Fig. 16 a typical record of the strain gage response and the attenuated crystal response obtained on a dual beam oscilloscope is shown. Now a number of crystal packages were constructed as shown in Fig. 11. However the lead wires were omitted and the packages were tested using the experimental arrangement shown in Fig. 17. The calibration technique was essentially the same as the previously established split Hopkinson bar technique reported in [1]. The piezoelectric constant was computed from the measurements. A typical record of the strain gage response and the attenuated crystal response is shown in Fig. 18. The interference of the crystal output with the strain gage output was eliminated by attaching the two bars together with epoxy, thus isolating the bar with the strain gage station from the transducer package. An average value of 1557 pcoulombs/Lb. was obtained for the

piezoelectric constant which compared with the published value of 1650 pcoulombs/Lb. for the PZT-5a ceramic crystal material, the order of agreement being the same as those obtained for quartz [1] and within manufacturer's tolerance. A limestone block with dimensions 15" x 15" x 11½" which was also used by Ricketts [2] for surface wave measurements was drilled as shown in Fig. 19. Four transducer packages were assembled and inserted in the 3/16" diameter holes again using wax as the bonding agent between the bars and the rack material. The experimental arrangement is shown in Fig. 20. The free surface was loaded by shooting 3/16" diameter balls with an air gun through an 1/8" diameter loading bar. The loading pulses were measured by means of both x-cut quartz crystals and PZT-5a crystals at the contact point as shown in Fig. 20. Both voltage amplification and charge amplification were adopted to measure the crystal responses inside the block. Typical input and output pulse shapes are shown in Fig. 21(a) for a sphere impact as shown in Fig. 21(b). Similarly a number of measurements were made for different impact locations. Each crystal station measures the unidirectional stress in the direction of the crystal axis i.e. in the direction of the bar. For example, referring to Fig. 19, station 1 measures σ_{zz} and stations 2 and 3 measure σ_{xx}. The various pulse shapes and the corresponding input pulse shapes and impact locations are shown in Figs. 22 to 29*. A comparison of the properties of limestone and magnesium is given in Table 2.

Presently the experimental results are being compared with the results obtained from a finite element program.

*Table 3 shows a summary of stresses measured and appropriate scale factors for the various pulse shapes

MATERIAL	DENSITY ρ Lbf/in^3	ROD WAVE VELOCITY c_o ins./sec.	SPECIFIC ACOUSTIC IMPEDANCE ρc_o $Lb\text{-}sec/ft^3$	MODULUS OF ELASTICITY E_{psi}	DYNAMIC POISSON'S RATIO ν	REFERENCE
Magnesium	0.0628	195,000	54,800	6.32×10^6 Dynamic (compressive)	--	Experimentally determined
Glass	0.108	190,000	91,800	9.0×10^6	--	Materials of High Vacuum Technology by W. Espe Pergamon Press, 1966
Ceramic PZT-5a	0.2782	103,400	128,600	7.7×10^6	--	Veritron Bedford, Ohio Data Sheet
Ceramic PZT-4	0.2746	116,400	142,900	9.57×10^6	--	"
Limestone	0.0805	141,400	51,100	4.3×10^6 to 6.1×10^6	0.27 to 0.31	Communicated by Dr. Ricketts
Yule Marble	0.101	Reference [2] and Section (c)- present report				

TABLE 2

Run No.	Impact Location	Input						Output - PZT-5a Crystal Transducers						
		Fig. No.	Crystal Material	Method of measurement	Details of measurement	Capacitance μμF	Scale Factor	Station No.	Fig. No.	Stress designation	Method of measurement	Details of measurement	Capacitance μμF	Scale Factor psi/div.
1	P1	21(a)	x-cut Quartz	charge amplification Kistler Model 568	Cal Factor 1.02 Range 1mv/lb. 0.5 v/div	--	50 lb/ div	1	21(a)	σ_{zz}	charge amplification ENDEVCO Model 2710	Transducer Sensitivity 10 Range 10 0.5v/div.	--	-26.2
5	P2	24	PZT-5a	Voltage amplification	100 x 5v/div.	204	64.2 Lb/ div.	1	25	σ_{zz}	Voltage amplification	0.2v/div.	374	+3.91
								2	24	σ_{xx}		0.2v/div.	334	+3.49
								3	26	σ_{xx}		0.1v/div.	611	+3.2
7	P3	27	PZT-5a	Voltage amplification	100 x 5v/div.	204	64.2 Lb./ div.	1	28	σ_{zz}	Voltage amplification	0.1v/div.	374	-1.96
								2	27	σ_{xx}		0.1v/div.	334	-1.75
								3	29	σ_{xx}		0.1v/div.	611	-3.2

TABLE 3

A plexiglass model of the Yule marble block currently in hand was made. The optimum locations of the crystal transducer packages in the rock are being determined using this model in conjunction with the analytical results. The drilling of the rock and embedding of crystals will commence soon. The actual drilling will be done at right angles to the surfaces of the block which has been determined by the choice of a rectangular coordinate system for the location of the transducer packages. Since the PZT-5 crystals are highly sensitive, it had been decided to use 1/16" diameter x 0.020" thick crystals with 1/8" diameter bars. These transducer packages are being constructed. The calibration of these packages will be completed shortly. These smaller diameter transducer packages will be used in Yule marble blocks thus reducing the possibility of altering the wave processes due to the insertion of metal bars in rock like material.

The following is the approximate schedule of endeavors planned for the rest of the contract period: (1) The construction and calibration of the 1/8" dia. transducer packages which is expected to be completed by the end of September 1972. (2) The drilling of one Yule marble block and mounting of these transducer packages in the block which will be completed by the middle of November 1972 (3) The actual measurements of body waves in the Yule marble block using essentially the methods of impact and measurement used already for the Limestone block which will be completed by the end of Dec. 1972. (4) The repetition of body wave measurements in the second Yule marble block, making any necessary changes in the location of the transducers

and in the methods of measurements, which is planned for completion in Jan. 1972. (5) Further investigation of surface wave measurements using the second Yule marble block which will be completed by the end of February 1972. (6) The comparison with the finite element method of solution and integral transform analysis will be pursued concurrently.

(c) Experimental Determination of the Physical Properties of Yule Marble under Static and Dynamic Loading

Introduction

As expressed in the previous technical report, the overall objective of this phase of the investigation consists of the determination of the geometric and mechanical properties of Colorado Yule marble, including fracture properties, aa a function of strain rate. Up to the time of publication of the previoua report, the following had been accomplished:

1. the axis of elastic symmetry (AES) of a slab of marble was determined using cryatallographic techniquea
2. a method of obtaining intermediate strain ratea of 10 to 100 aec^{-1} was obtained
3. the mechanics of rock coring and apecimen preparation were mastered
4. the aet up and calibration of instrumentation necesaary to record stresa-atrain relationahins at varioua atrain rates was accomplished
5. some preliminary mechanical pronerties were obtained.

Thia report details the progreas from that point.

Objectives

During the last six months the following objectives were accomplished:

1. the determination of the AES of a new alab of Yule marble used in the extenaive testing of the rock, and, the verification of

the AES in the block used by Ricketts [2]. Both of these studies were performed using the optical crystallographic technique described in the previous technical report.

2. the determination of the static and dynamic elastic constants for Yule marble
3. the investigation of fracture stress versus strain rate and specimen orientation for both tension and compression.

In addition to these objectives, some additional subdivisions of the testing program, to be completed in the next 6 month period, are described:

4. the characterization of the nonlinear and/or non elastic behavior of the rock
5. in order to get dynamic fracture strengths, a split Hopkinson bar will be used with a reduced and specially contoured rock midsection. This procedure should allow for the construction of a dynamic stress-strain curve to fracture for both tensile and compressive pulses.
6. the characterization of the failure process in terms of the strain rate parameter, including optical observations of the phenomena. From this information, a comprehensive model of the mechanical response of the substance may be solved.

Methodology and Procedure

Previous experiments on the first marble slab obtained from the Clervi Marble Co. are described in the last technical report [1]. It was found using crystallographic methods that the AES of this slab

was neither in the slab nor perpendicular to it but rather at an inconvenient angle. For that reason, a new slab was sought and obtained, again from the Clervi Marble Co. of San Francisco. The manner in which the test specimens were cut from this slab is shown in Fig. 30. The AES of the slab lay in the plane of the slab and was determined both by visual inspection of the distinct bedding planes and by crystallographic techniques. The orientation of the optic axis of 100 crystals of a specifically prepared thin section is shown graphically in Fig. 31. The thin section was cut so that the orientation of the AES as deduced from visual inspection of the bedding planes (assuming the AES is perpendicular to these planes) is normal to the slide surface.

Compression specimens measuring 1.05 inches in diameter and of lengths between 1.4 and 2.2 inches were cored using an oil cooled diamond bit. The ends of these specimens were milled flat using a special jig and an oil cooled milling machine with a diamond abrasive surface. These surfaces were flat and parallel to 1/1000" and the lateral dimensions of each specimen at the ends of two mutually orthogonal diameters as well as the diameter of the specimen was recorded.

Specimens used for tensile testing and in the Hopkinson bar experiments were cored using a 7/8" O.D. diamond bit and cut on a water cooled gravity feed drill press especially converted for the coring of rock specimens. These cores measured ~ 3/4" diameter by nominally 6" in length and were cut nearly perpendicular at the ends using a diamond cut off saw at very slow feed rates (2"/hour).

Ten compression specimens were cut from each of three mutually orthogonal directions, X,Y,Z. The Z axis lies in the plane and the X axis is normal to the slab. Y and Z direction specimens were nominally 2.0 inches long, while the X direction specimens, owing to the thickness of the slab, measured roughly 1.4 inches.

These specimens were mounted with Baldwin-Lima-Hamilton FAE-12-12S9L epoxy backed strain gages of 120 Ω resistance having a gage factor of 2.01. These 1/8" gages were mounted longitudinally and diametrically opposed at the midsection of the specimen using EPY-150 epoxy. They were wired in series to eliminate the measurement of any bending component.

The gages were incorporated in an AC-excited bridge curcuit including an amplifier and the output was recorded on a plotter. The records were calibrated by means of known shunt resistances across the gage. The applied compressive force was determined by means of a calibrated 0-20,000 lb range Instron load call. Strain-time and stress-time records were recorded on a strip chart recorder. For the fastest of these quasistatic loading tests (less than 2 seconds duration) an oscilloscope was used to record both stress-time and strain-time data.

An Instron testing machine was used to load the specimens as shown in Fig. 32. A ball and socket loading member with a 3" diameter bearing plate and a 2" dia. ball assured uniform contact with the loading surfaces. A specimen of 7075 aluminum was mounted with longitudinal and transverse gages and tested. The data from these tests were reduced in a manner identical to that used for the rock specimens. The elastic constants obtained from this data were

$E = 11.6 \times 10^6$ psi and $\nu = .34$ as compared with the accepted values of $E = 10.6 \times 10^6$ psi and $\nu = .33$. Although there is some error in Young's modulus relative to the accepted value (< 10%), the value for Poisson's ratio agrees closely (<3%), and there is no hysteresis present.

In order to determine the static elastic constants of Yule marble, three compression specimens were prepared as above. The constitutive relation for a transversely isotropic material may be written in terms of well-known constants as follows:

Let the z direction be the AES and E', ν' be Young's modulus and Poisson's ratio in that direction. Let x and y denote coordinates lying in the plane of isotropy (PI). Let E and ν be the elastic constants in this plane. Let G' denote the shear modulus in any plane perpendicular to the PI. Then the constitutive equation is:

$$\epsilon_{xx} = \frac{1}{E}\left(\sigma_{xx} - \nu\sigma_{yy}\right) - \frac{\nu'}{E'}\,\sigma_{zz}$$

$$\epsilon_{yy} = \frac{1}{E}\left(\sigma_{yy} - \nu\sigma_{xx}\right) - \frac{\nu'}{E'}\,\sigma_{zz}$$

$$\epsilon_{zz} = -\frac{\nu}{E}\,(\sigma_{xx} + \sigma_{yy}) + \frac{1}{E'}\,\sigma_{zz}$$

$$\epsilon_{yz} = \frac{\sigma_{yz}}{G'}$$

$$\epsilon_{xz} = \frac{\sigma_{xz}}{G'}$$

$$\epsilon_{xy} = \frac{\sigma_{xy}}{G} = \frac{2(1+\nu)}{E}\,\sigma_{xy}$$

Using the specimens mounted with strain gages as shown in Fig. 33, all the elastic constants can be determined using these three specimens. They were tested in compression from 0-1200 psi at about 100 psi/sec loading rate for seven cycles and elastic constants were measured on this seventh cycle. The specimens were then tested at 0-6000 psi at 300 psi/sec for three more cycles and stress and strain data as a function of time was recorded.

An attempt has been made to obtain the same type of information as above for the rock in tension. Different geometries have been employed but none have been very successful. One series of tests were performed on rock rods glued to aluminum endcaps as shown in Fig. 45. The rock cores were glued to the aluminum endpieces in a V block using high strength Scotchweld Structural Adhesive. Strain gages were mounted at the midsection and tensile tests to fracture were performed at various strain rates for specimens oriented both in the Y and the Z directions. The results of these tests are given in the next section.

In order to measure the dynamic elastic constants for Yule marble, rock cores 3/4" ϕ x 6" ℓ were cut as described above. The ends of these rods were cut perpendicular using a diamond cutoff saw. Three rods, all with the same orientation, were glued together and mounted with strain gages as shown in Fig. 34. These strain gages were monitored by an oscilloscope through a dynamic bridge balance and calibrated using a known shunt resistance. Aluminum endcaps 1/2"ℓ x 3/4"ϕ were attached with wax to the impact end of the rod to prevent local fracturing. These specimens were held

vertically in a drop test set up as shown in Fig. 35. A 1/2" diameter ball was dropped from 22½" through an aligning tube onto the rock rod. Strain pulses were recorded at two stations, each using the same time base. The scope was triggered using a piezoelectric crystal taped to the side of the rod. This apparatus was to measure strain histories at three gage locations: two longitudinal strains and one transverse strain. Peak strain arrival times were used to calculate wavespeeds and these dynamic elastic constants using $E = \rho C_0^2$ for both tensile and compressive pulses. The ratio of transverse to longitudinal strain gave Poisson's ratio in those tests. In order to ascertain the error in this setup, the dynamic elastic constants of a rod of 7075 aluminum with the same dimensions as the rock rod was used. For this rod, wavespeeds of 200,000 in/sec implying $E = 10.2 \times 10^6$ psi were obtained for both tensile and compressive pulses. Poisson's ratio obtained was .335.

Results

Ten compressive specimens in each of three mutually orthogonal directions X,Y and Z were cut and instrumented as described in the previous section. Two specimens from each direction were tested at each of five strain rates and both stress-time and strain-time data to fracture were gathered. From these data stress-strain curves were constructed. The general shape of the stress-strain curve in each direction does not seem to depend on strain rate. Figures 36, 37, 38 show the two most deviant curves from each of the three directions.

The shape of the stress-strain curve is both characteristic with respect to specimen orientation and reproducible. Initially, there is a region of increasing stiffness from an initial tangent modulus E_1 to a region of constant modulus E_2. This stiffening region where $\frac{d^2\sigma}{d\epsilon^2} > 0$ persists until roughly one third the maximum stress σ_m is reached. The material exhibits constant modulus E_2 between $\frac{\sigma_m}{3}$ and $\frac{2\sigma_m}{3}$ and with increasing stress enters a region of decreasing tangent modulus, $\frac{d^2\sigma}{d\epsilon^2} < 0$. Directly preceeding failure, the modulus becomes negative and the material fails at a value of fracture stress σ_f lower than σ_m. Figure 39 indicates the values of E_1 and E_2 for the specimens tested. Due to low amplifications of both stress and strain signals near the origin, error in the determination of E_1 is estimated at around $\pm 20\%$ of the actual value. This modulus is obtained with greater accuracy in subsequent tests. Strain rates for these tests were calculated on the basis of $\frac{\text{strain}}{\text{time}}$ at $\frac{2\sigma_m}{3}$. Strains become large as failure approaches giving increasing strain rates near fracture.

In the region near fracture, strain recorded by the gages no longer is an accurate measurement of average cross-sectional specimen strain. Fracture paths initiate, almost without exception, at the corners of the specimens and travel diagonally through producing one plane of failure. In X and Y oriented specimens, these planes were invariably oriented such that their normal lay in the plane produced by the test axis and a point lying on the AES or Z direction. Gages mounted such that this plane of failure traveled through them produced larger strain readings than those located away from the fracture

path. This conclusion was reached after mounting four gages at 90° intervals around both Y and Z direction specimens and comparing σ- ϵ curves produced by gages through which the fracture path occurred with those produced by gages distant from this path. The results of this test are shown in Fig. 40. Specimens in the X direction were unintentionally mounted so that the fracture path was as far as possible from the gage while specimens in the Y were mounted such that the fracture path always passed through the gages. Thus, the apparent difference in material properties near failure, X direction specimens appearing brittle while Y direction specimens showing remarkable amounts of seemingly near plastic strain, is explained. Figure 40 clearly indicates how the structure of the material is such that the assumption of one-dimensionality breaks down near failure.

Specimens in the Z direction show no preference in fracture plane orientation, although they also split diagonally, sometimes accompanied by secondary cracks initiating at the bearing plates and running parallel to the specimen axis. In the four gage test, there was very little difference in strain between two sets of gages even though the fracture path lay clearly through one set.

Maximum stress σ_m as a function of static strain rate and direction is shown in Fig. 41. No strong strain rate dependence is evident for either the X or Y directions. Z shows s greater dependence of maximum stress with $\log_{10}\dot{\epsilon}$. The difference in σ_m for X and Y directions may be attributable to shorter (1.4" vs. 2.0") X direction specimens.

The results of the compression tests used to obtain the static elastic constants are shown in Fig. 42. As is evident from these figures, more of these "constants" are truly constant. Previous tests on this material have shown a permanent deformation accompanying each virgin stress level. On repeated loading to this stress level, the stress-strain curve exhibits hysteresis but no appreciable permanent set after this first cycle. In order to avoid measuring any "first cycle" effects, the specimens were all loaded through six cycles before the stress-strain relationships were recorded on the seventh. The following elastic constants were determined:

$$E_1 = 4.7 \times 10^6 \text{ psi}$$

$$\nu_1 = .13$$

$$E_1' = 2.3 \times 10^6 \text{ psi}$$

$$\nu_1' = .05$$

$$G_1' = 2.8 \times 10^6 \text{ psi}$$

These same specimens were then loaded through three additional cycles at 300 psi/sec to 6000 psi. A typical result of these tests is shown in Figs. 43, 44. As can be observed from the figure, an initial permanent deformation occurs after the first loading cycle. Subsequent loading cycles show only minor amounts of permanent deformation after each cycle, while retaining a nonlinear form at low stresses. Hysteresis in the second and third cycles is greatly reduced. Again, there exists a region between $\sigma_m/3$ and $2\sigma_m/3$ of very nearly constant modulus.

Several preliminary tests have been performed to try to indicate the viscoelastic nature of the rock, if any. Creep tests at stresses up to $\frac{2\sigma_m}{3}$ seem to yield little viscoelastic phenomena in the 1-1800 sec range. Some definite creep is observed for Y compression specimens at about 7/8 σ_m but this data is still preliminary in nature.

Dynamic elastic constants were obtained by measuring strain-time histories at two longitudinal and one transverse station in base oriented in each of the three directions Y, Z and 45° . These tests produced the following dynamic elastic constants:

	compressive pulse	tensile pulse
E	11.3×10^6 psi	11.3×10^6 psi
ν	.29	.24
E'	5.0×10^6 psi	3.2×10^6 psi
ν'	.13	.09
G'	-	-

Although the value of G' has not been calculated as yet, the procedure is straightforward and enough data is available in terms of five dependent tests to obtain five elastic constants. This method of measuring the elastic constants is identical with the method used in the static compression tests in so far as location of recording gages with respect to X, Y, and Z directions is concerned. The following relations were used

$$E' = \rho C_{0_Z}^2 \qquad \nu' = -\frac{\epsilon_{xx}}{\epsilon_{zz}} \qquad \text{Z-axis bar}$$

$$E = \rho C_{0_Y}^2 \qquad \nu = -\frac{\epsilon_{yy}}{\epsilon_{xx}} \qquad \text{Y-axis bar}$$

Wavespeed and a Poisson's ratio have been obtained for the 45° specimen and thus a dynamic G' can be determined. These elastic constants were measured at peak longitudinal strains of less than 200 μin/in and thus fall into the initial elastic region as determined by the static tests. As indicated by Ricketts' [2], conversion of these technical constants to corresponding velocity constants is straightforward.

Some problems were encountered in the development of a satisfactory method of testing the rock in tension. An initial tensile specimen design was patterned after standard metal test specimen geometries and loaded by means of a friction hold with end clamps as shown in Fig. 45. These specimens broke as they were being attached to the testing machine.

A second geometry was considered. Rock slabs measuring 6" x 1½" x 1/4" were attached to aluminum end pieces 3" x 1½" equipped with a ½" diameter loading hole using Scotchweld Structural Adhesive. Load was applied through a chain so that if the specimen and endcaps arrangement was symmetrical with respect to a line between the loading holes, no bending moment could be introduced. These specimens proved unsatisfactory as they consistently broke at the rock-aluminum interface. In addition, these specimens were extremely difficult to fabricate and align properly. In order to get some indication of the strain

state in the rock, a brittle coating, Stress Coat, was applied to the rock surface. At room temperature this material cracks near 500 μin/in, although using special techniques to cool the coating, this limit can be lowered to 200 μin/in. Even in the region directly adjacent to the tensile fracture path, only very few cracks in the Stress Coat were observed. Maximum tensile strain at failure in Yule marble is about the same as that required for crack initiation of the Stress Coat and thus this brittle coating is not very useful in obtaining an overall prefracture strain state necessary in order to detect stress concentrations. A third specimen geometry was decided on, primarily because of ease of fabrication. This tensile test consisted of 6" long 3/4" diameter rock rods glued with Scotchweld Structural Adhesive to threaded aluminum end caps as shown in Fig. 45. The ends of the rods were cut nearly perpendicular to the axis using a diamond cut off saw. The endcaps were wrapped with transparent tape until they measured within .002 of the diameter of the rock rods. The endcaps were glued to the rock by placing the pieces in an aluminum L member. Weights were applied to the rod and endcaps to assure that they remained securely in the bottom of the L as shown in Fig. 46.

These specimens were mounted with diametrically opposed longitudinal strain gages located at the midsection of the rock. Four specimens in both the Y and Z directions were prepared in this manner.

The rock tensile specimens were tested at four different loading rates to fracture and the resultant stress-strain curves are shown in Figs. 47 and 48. All of the Y direction specimens broke at the

rock-specimen interface. The stress-strain curves obtained from these tests are probably in error in three ways. First, the strain measured by the gages is probably much smaller than that at the rock-aluminum interface where failure eventually occurred. Second, fracture stress is underestimated since a stress concentration apparently exists at the interface. Third, the apparent increase in fracture stress with respect to strain rate may be partially due to a strain rate property of the glue and thus a strain rate sensitivity of the stress concentration. Specimens oriented in the Z direction are also subject to these criticisms but to a lesser extent as two of the four specimens broke relatively near the gages.

The specimen geometry for tension is not considered satisfactory. Now in progress is an attempt to fabricate a reduced section contour from 6"ℓ x 3/4" $\varnothing$ rods. This configuration should eliminate distal fractures. However, affects of additional machining of the rock must be investigated.

CONCLUSIONS

After one and one-half years of theoretical and experimental investigation involving the propagation of body and surface waves in a transversely isotropic natural rock, namely Yule marble, the following results and conclusions can be summarized:

(1) An analysis has been developed based on integral transform procedures utilizing the Cagniard de-Hoop technique of inversion for the propagation of waves in a transversely isotropic half-space with the axis of symmetry lying in the free surface when subjected to an arbitrary concentrated normal force. This model simulates the normal impact of a sphere on a large block of Yule marble as represented by corresponding experimental conditions. The displacements, strains and stresses produced by body waves in the interior of the medium have been completely delineated, and numerical results have been obtained specifically for a step input and a sine-squared input in time; the latter is one of the best simple analytical representations of an actual impact by a sphere. The formulation for the surface response has been completed and the procedure for obtaining numerical results has been initiated; however, computational difficulties have been encountered at singular points of the solution and attempts are currently under way to resolve this problem.

(2) A finite-element program for the identical problem was evolved approximately five months ago, but has since been refined and improved, although requiring further checking. Typical numerical difficulties are encountered when results are desired close to the source, requiring for its improvement very fine mesh sizes leading to extensive computational efforts.

(3) Complete transducer packages for the direct measurement of dynamic stress components in the interior of rock and ceramic-type materials have been developed and externally calibrated both by means of split Hopkinson bars and embedment within rock bars. Drilling and insertion techniques have been evolved and applied to rods and blocks composed of nearly isotropic rock. Techniques are currently being constructed for in situ calibration of these packages in the interior of anisotropic rock masses.

(4) In the area of the determination of mechanical properties of the marble, the axes of elastic symmetry of static and dynamic test specimens as well as of the blocks to be used in the body wave experiments have been crystallographically determined. A large number of quasi-static and some dynamic tests have been performed both in tension and compression for various orientations of the material. Creep, cyclic loading and fracture studies have also been executed, and dynamic elastic constants have been determined for the material.

During the remainder of the contract period, it is expected to complete the analytical and experimental studies of body wave response and to compare the integral transform, finite-element and experimental results as a test of the validity of the model and the theoretical and test techniques employed. The characterization of selected mechanical properties of the Yule marble both under static and dynamic conditions is anticipated to be largely complete with the exception of fracture initiation and propagation studies that will require further effort.

The analytical procedures developed will permit ready extension to other classes of substances, such as orthotropic materials, while the techniques involving the construction and embedment of transducer packages will find wide applicability in the study of dynamic processes in the interior of large blocks or structural elements.

BIBLIOGRAPHY

1. Goldsmith, W., and J. L. Sackman, "Wave Propagation in Anisotropic Rocks," Annual Technical Report Number One, Feb., 1972. Contract H0210022 Bureau of Mines. University of California, Berkeley, Feb. 1972.

2. Ricketts, T. E., "Spherical Impact on an Anisotropic Half-Space," Ph.D. thesis, University of California, Berkeley, 1970.

3. Buchwald, V. T., "Rayleigh Waves in Transversely Isotropic Media," Quart. J. Mech. Appl. Math., Vol. 14, pt. 3, 1961.

4. Paradis, A. R., and Hussey, D. F., "Graphical Display System," Computer Center, Univ. of Calif., Berkeley, Apr., 1969.

5. Lion, K. S., Instrumentation in Scientific Research; Electrical Input Transducers, New York, McGraw-Hill, 1959.

6. Mason, Warren P., Physical Acoustics, Principles and Methods, Volume I - Part A, New York, Academic Press, 1964.

FIGURES

List of Figures

List of Figures

List of Figures

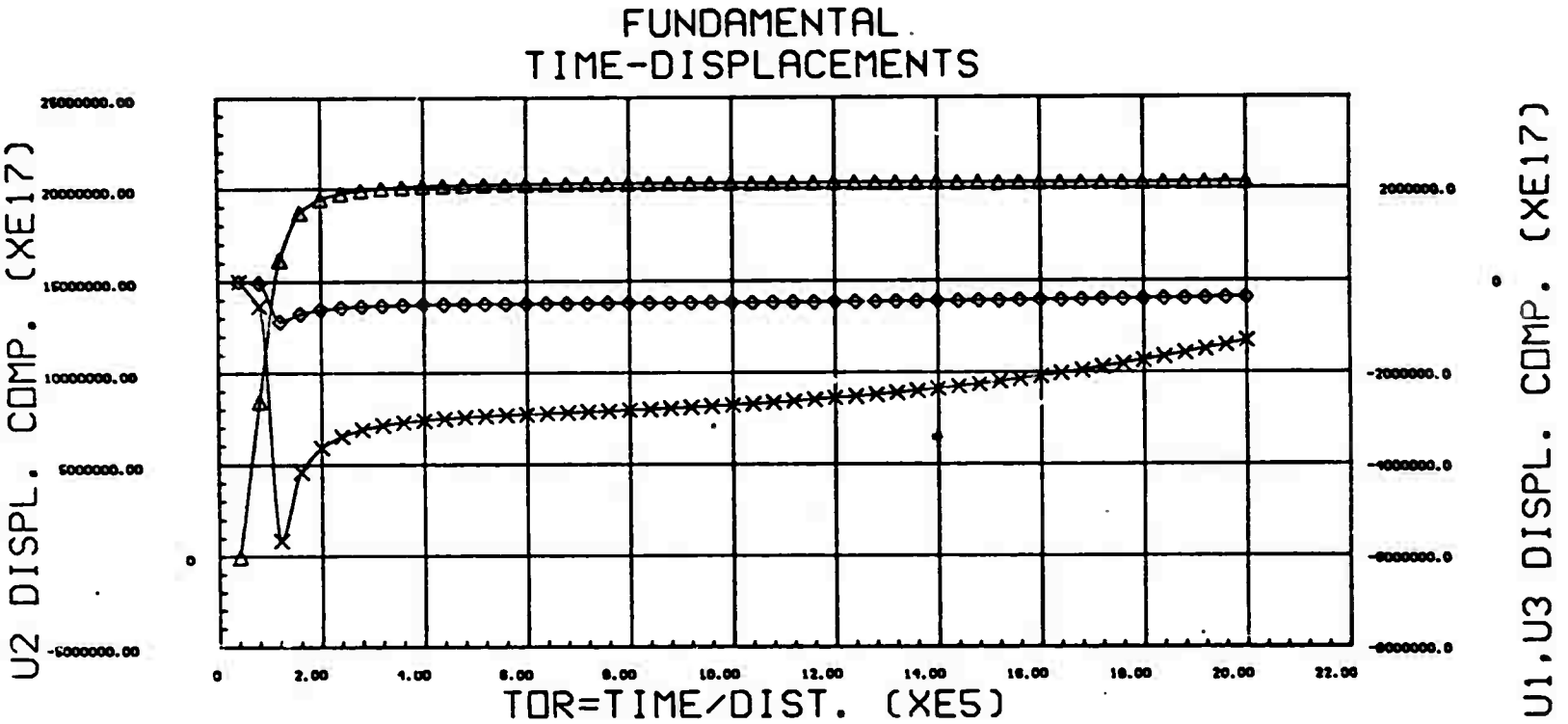

XU3 DISPL. COMP.
ΔU2 DISPL. COMP.
◇U1 DISPL. COMP.

Fig. 1

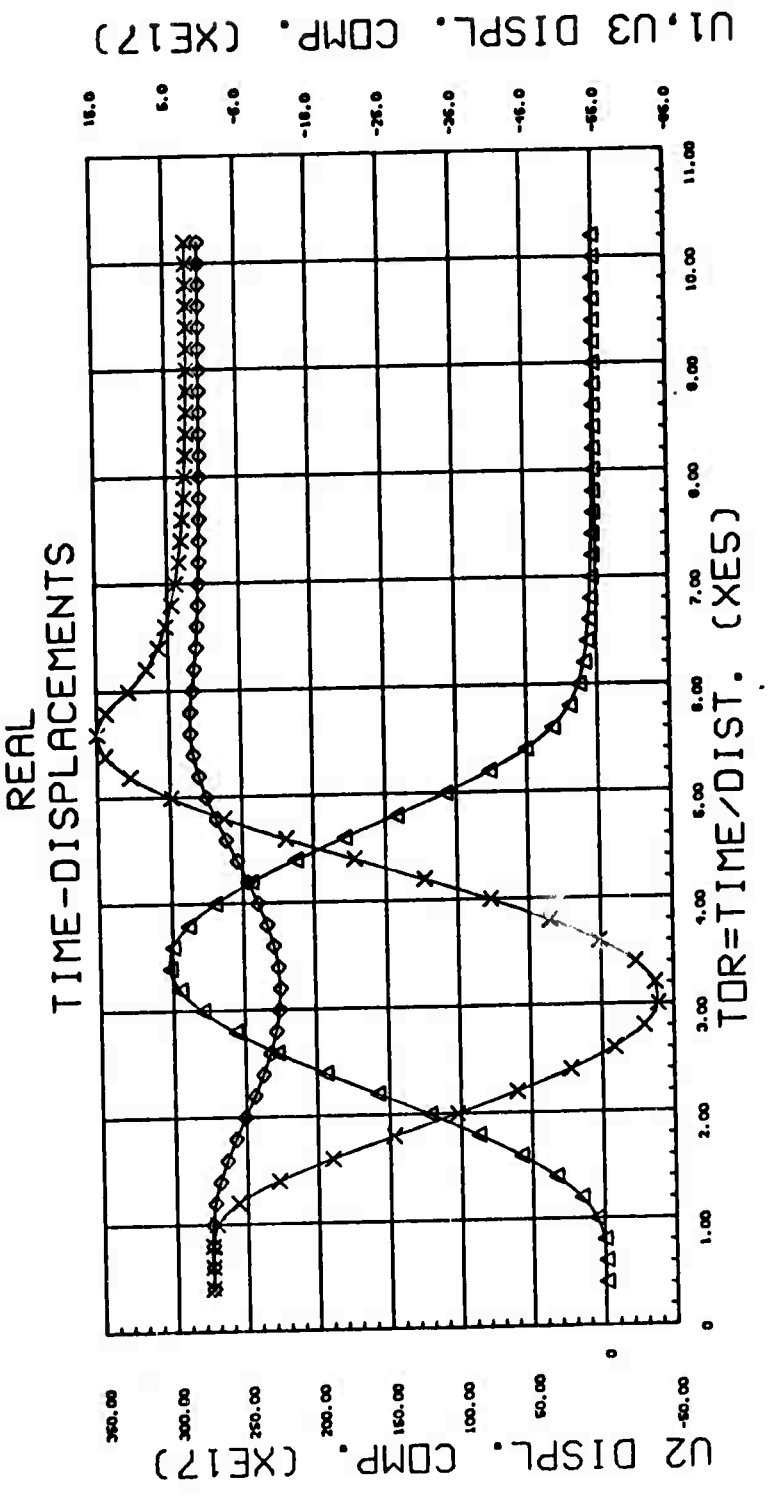
REAL
TIME-DISPLACEMENTS
U2 DISPL. COMP. (XE17)
U1,U3 DISPL. COMP. (XE17)
TOR=TIME/DIST. (XES)
XU3 DISPL. COMP.
ΔU2 DISPL. COMP.
◇U1 DISPL. COMP.

Fig. 2

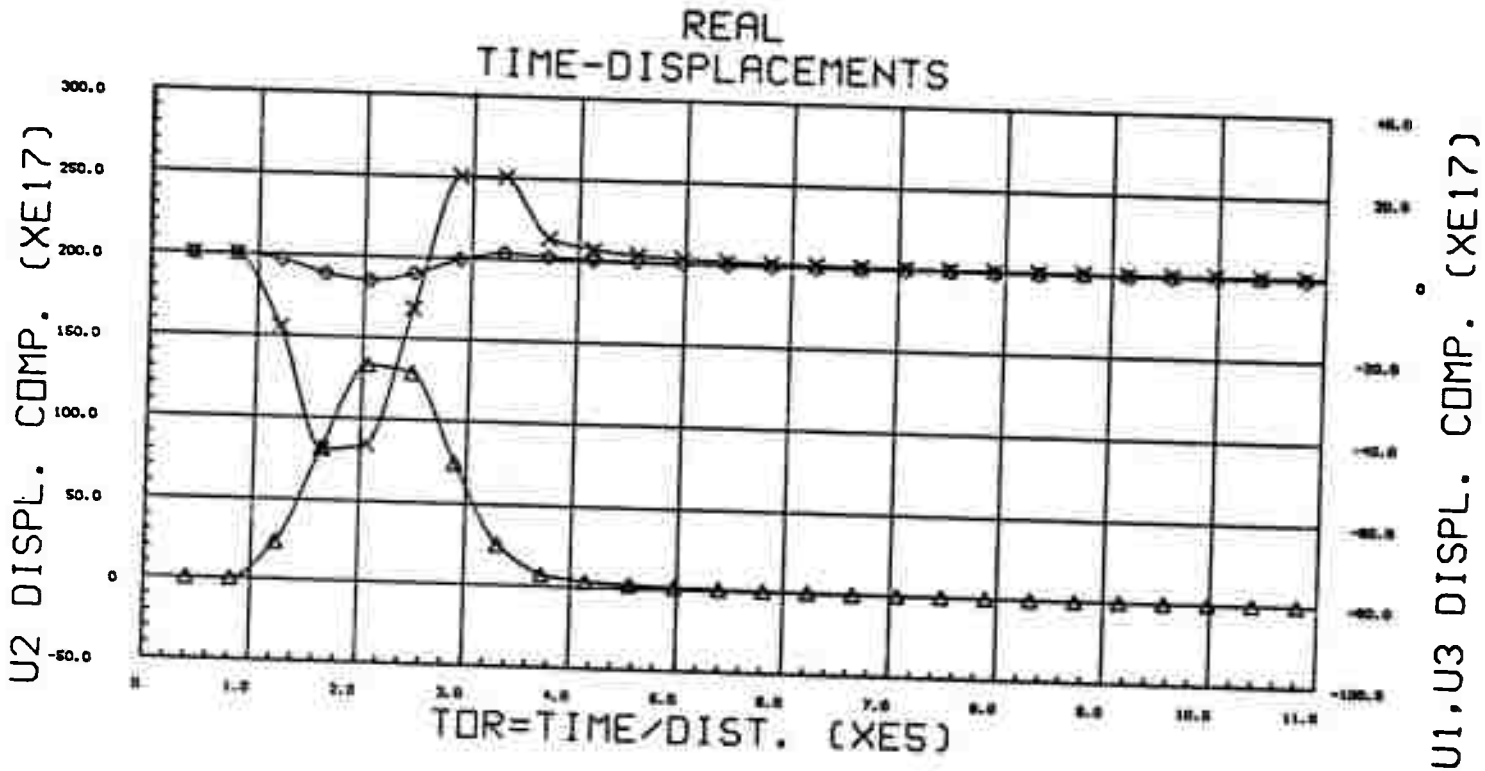
REAL
TIME-DISPLACEMENTS
U2 DISPL. COMP. (XE17)
U1,U3 DISPL. COMP. (XE17)
TOR=TIME/DIST. (XE5)
300.0
250.0
200.0
150.0
100.0
50.0
0
-50.0
XU3 DISPL. COMP.
ΔU2 DISPL. COMP.
◇U1 DISPL. COMP.

Fig. 3

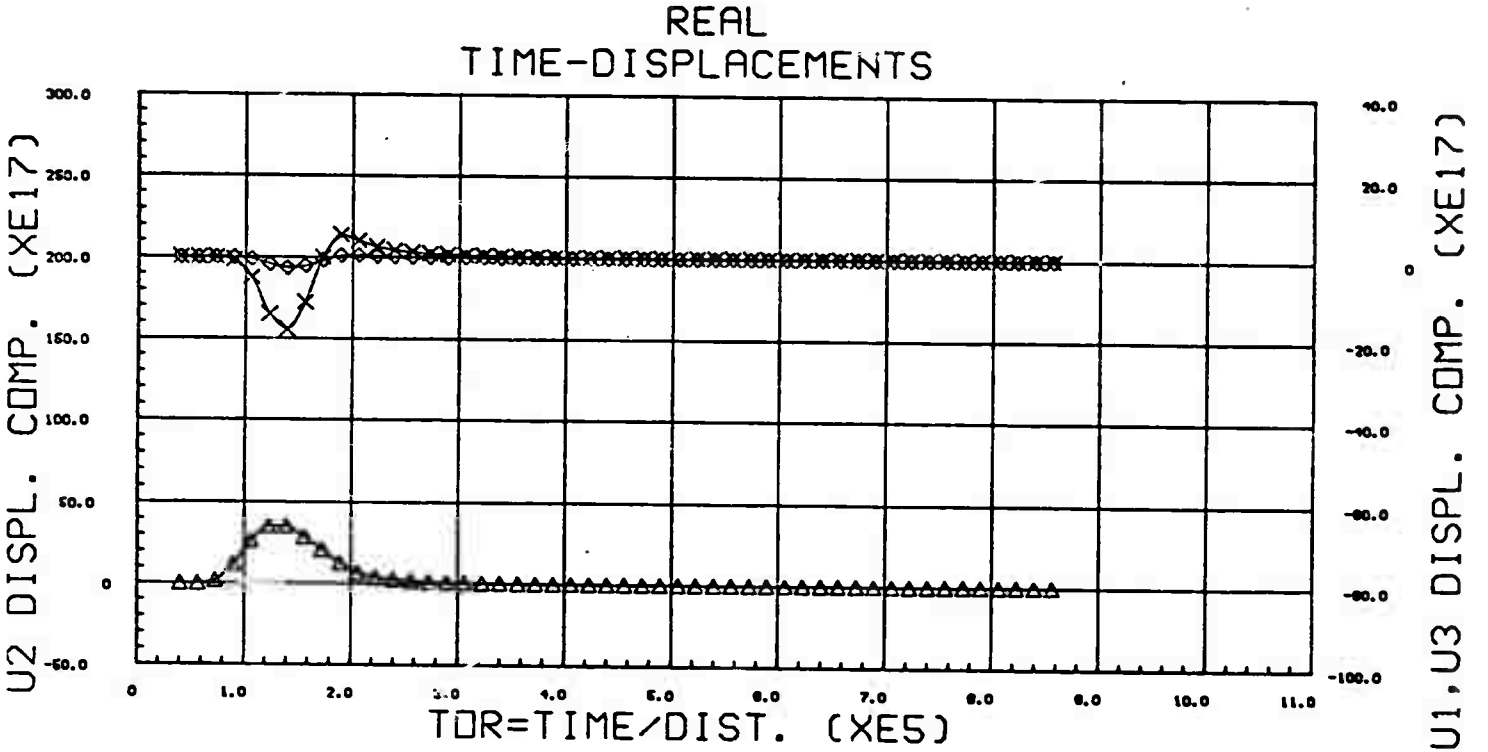

XU3 DISPL. COMP.
ΔU2 DISPL. COMP.
◇U1 DISPL. COMP.

Fig. 4

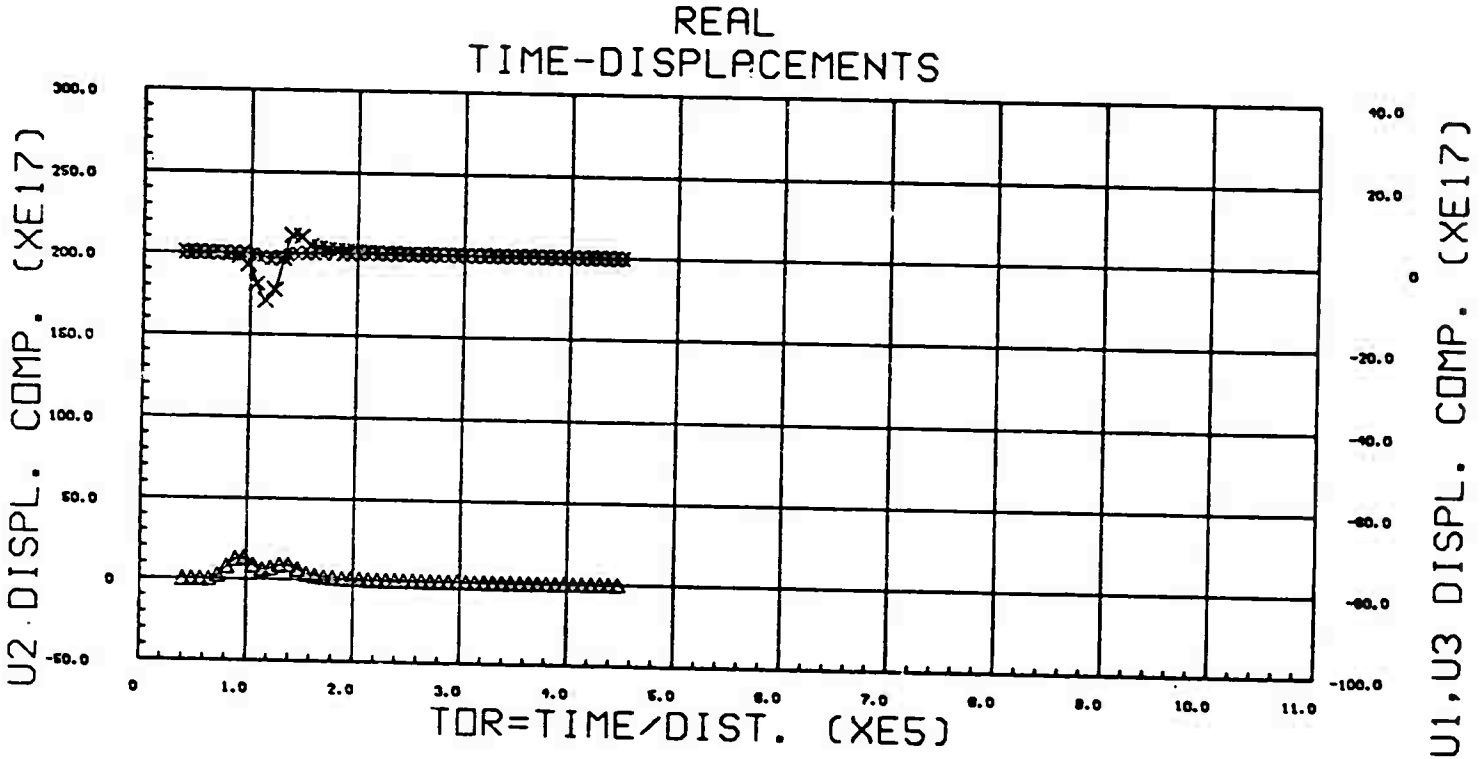

XU3 DISPL. COMP.
ΔU2 DISPL. COMP.
◇U1 DISPL. COMP.

Fig. 5

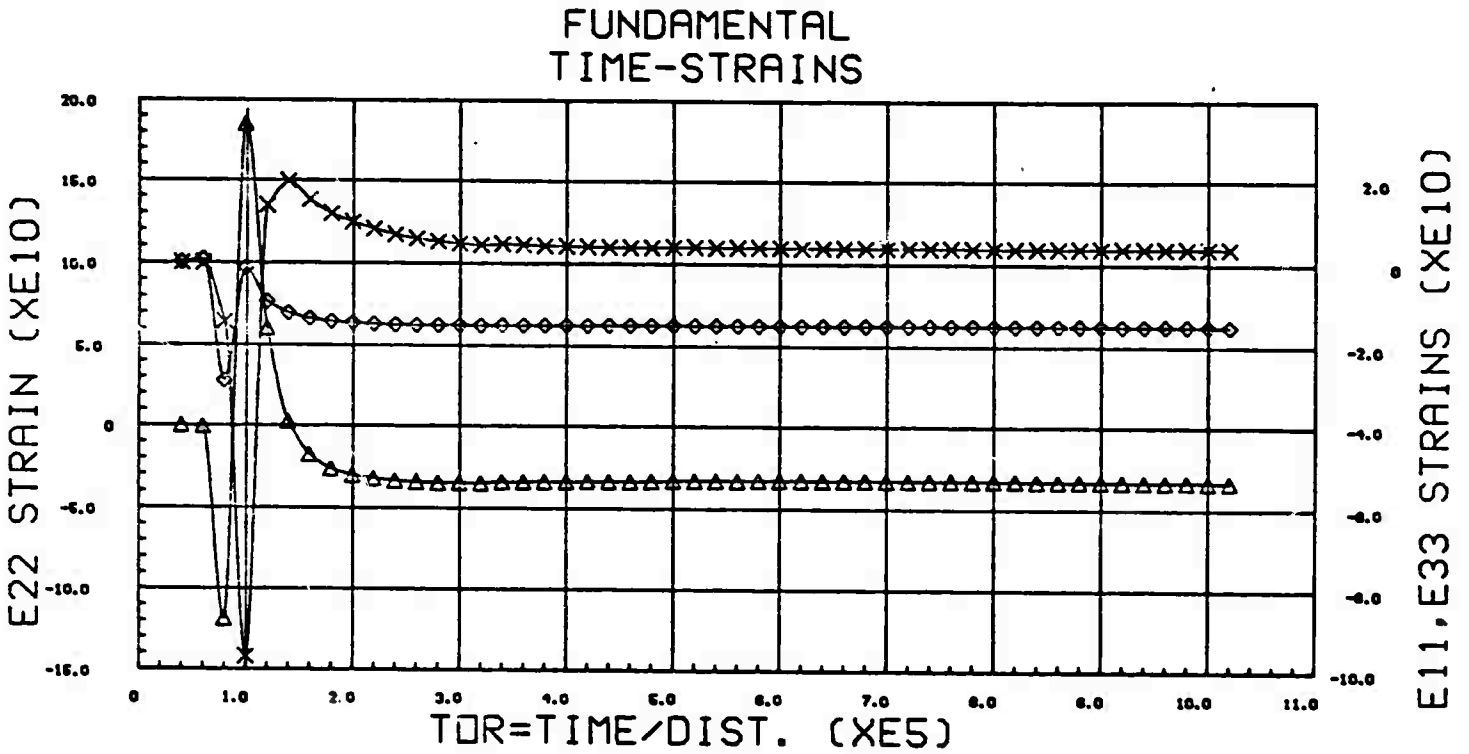

XE11 COMP.
ΔE22 COMP.
◇E33 COMP.

Fig. 6

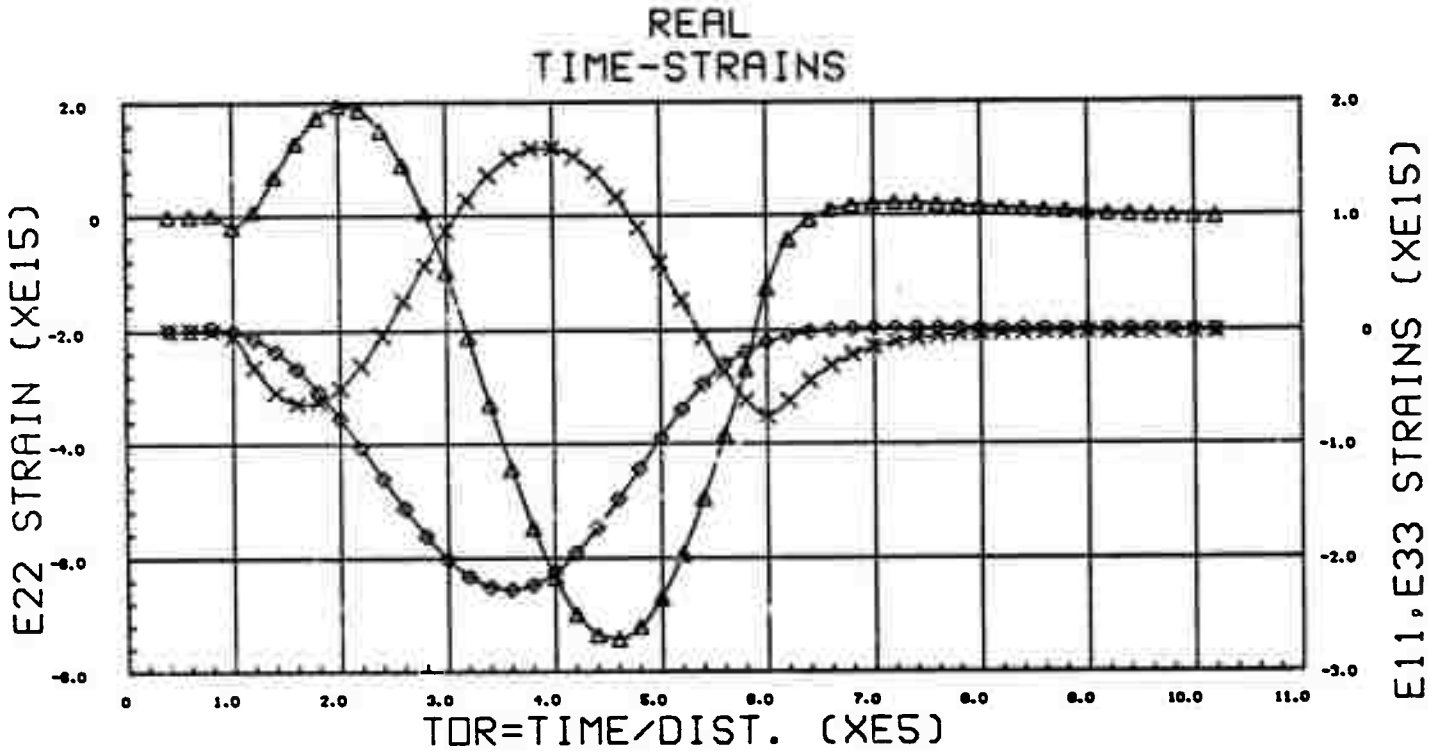

XE11 COMP.
ΔE22 COMP.
◇E33 COMP.

Fig. 7

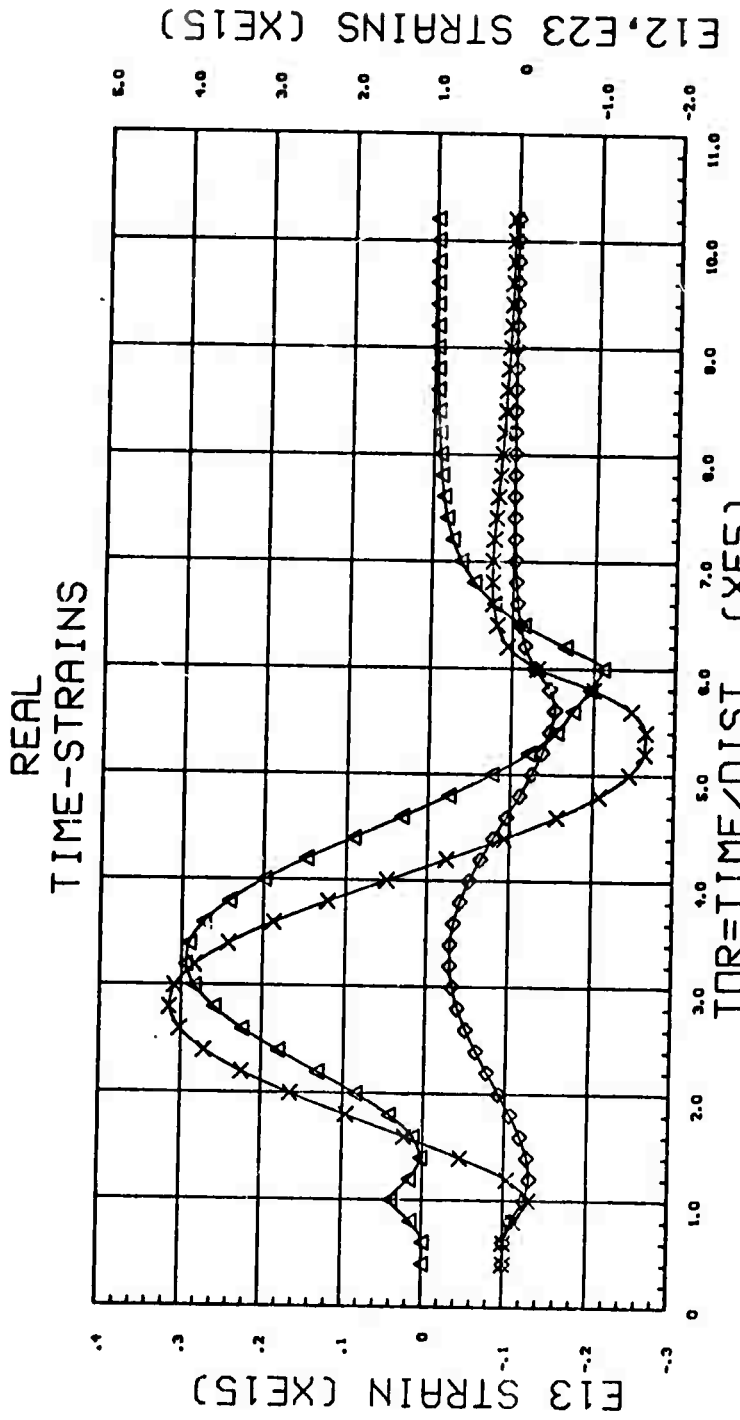
REAL
TIME-STRAINS
E13 STRAIN (XE15)
E12,E23 STRAINS (XE15)
TOR=TIME/DIST. (XES)
XE12 COMP.
ΔE13 COMP.
◇E23 COMP.

Fig. 8

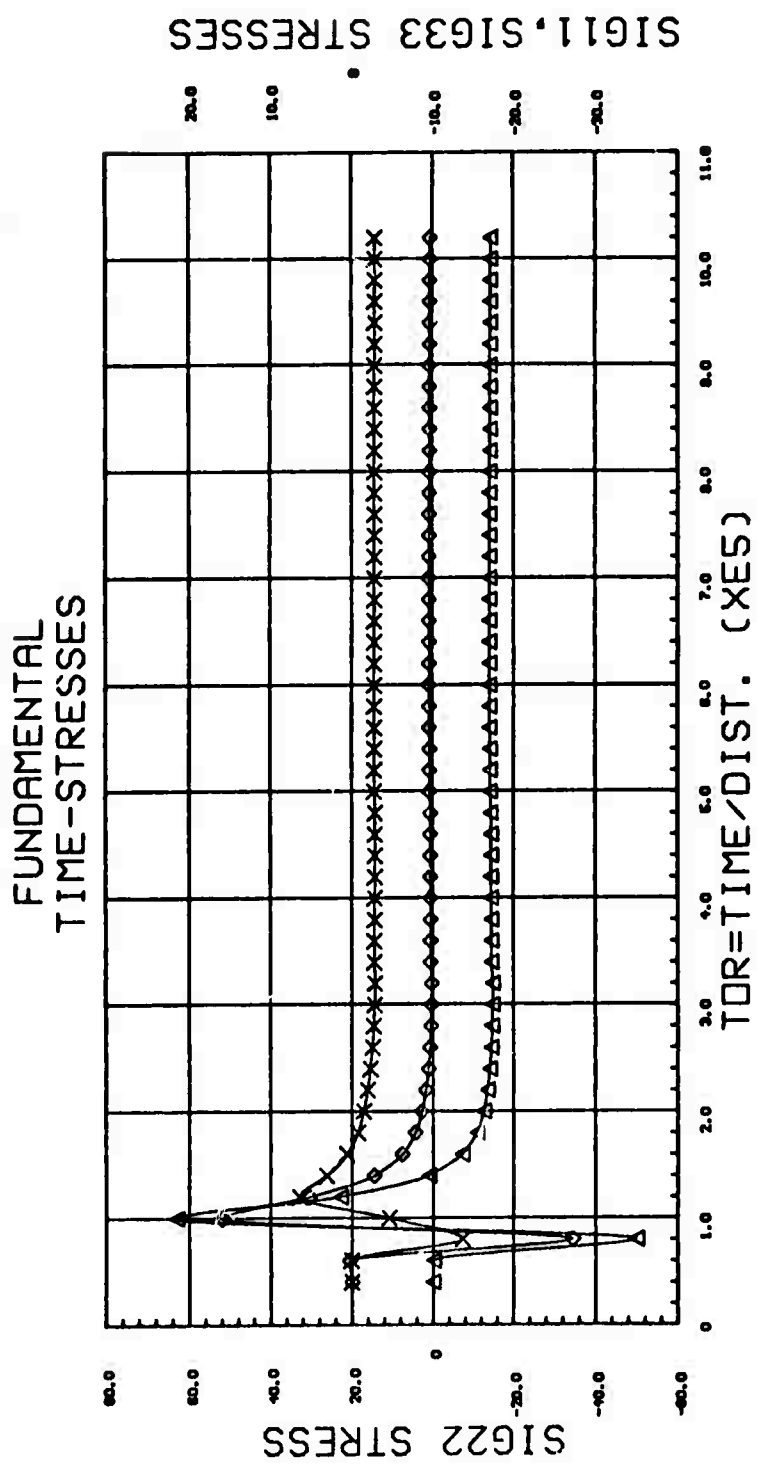
FUNDAMENTAL
TIME-STRESSES
SIG11,SIG33 STRESSES
SIG22 STRESS
TOR=TIME/DIST. (XES)
XSIG11 COMP.
ΔSIG22 COMP.
◇SIG33 COMP.

Fig. 9

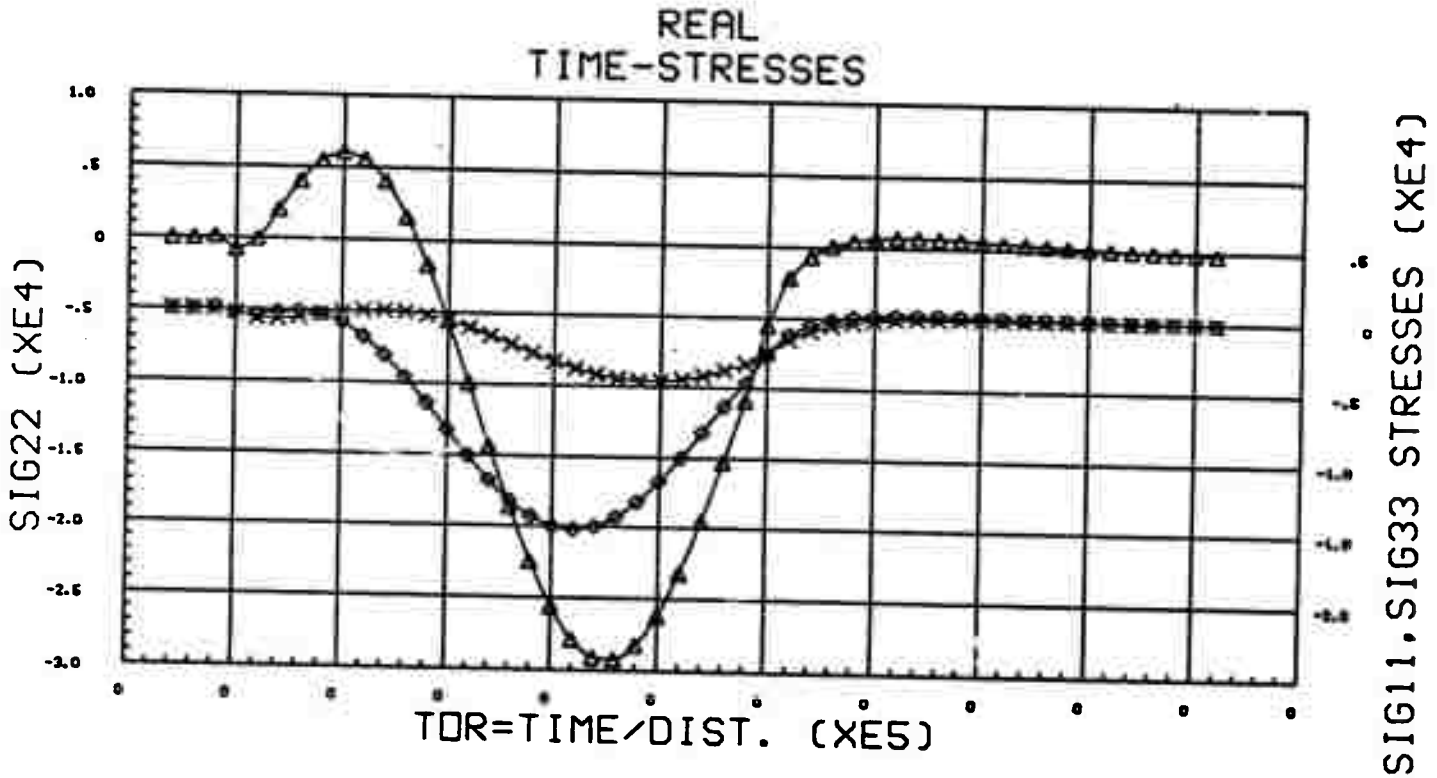
REAL
TIME-STRESSES
SIG22 (XE4)
SIG11,SIG33 STRESSES (XE4)
TOR=TIME/DIST. (XE5)
XSIG11 COMP.
ΔSIG22 COMP.
◇SIG33 COMP.

Fig. 10

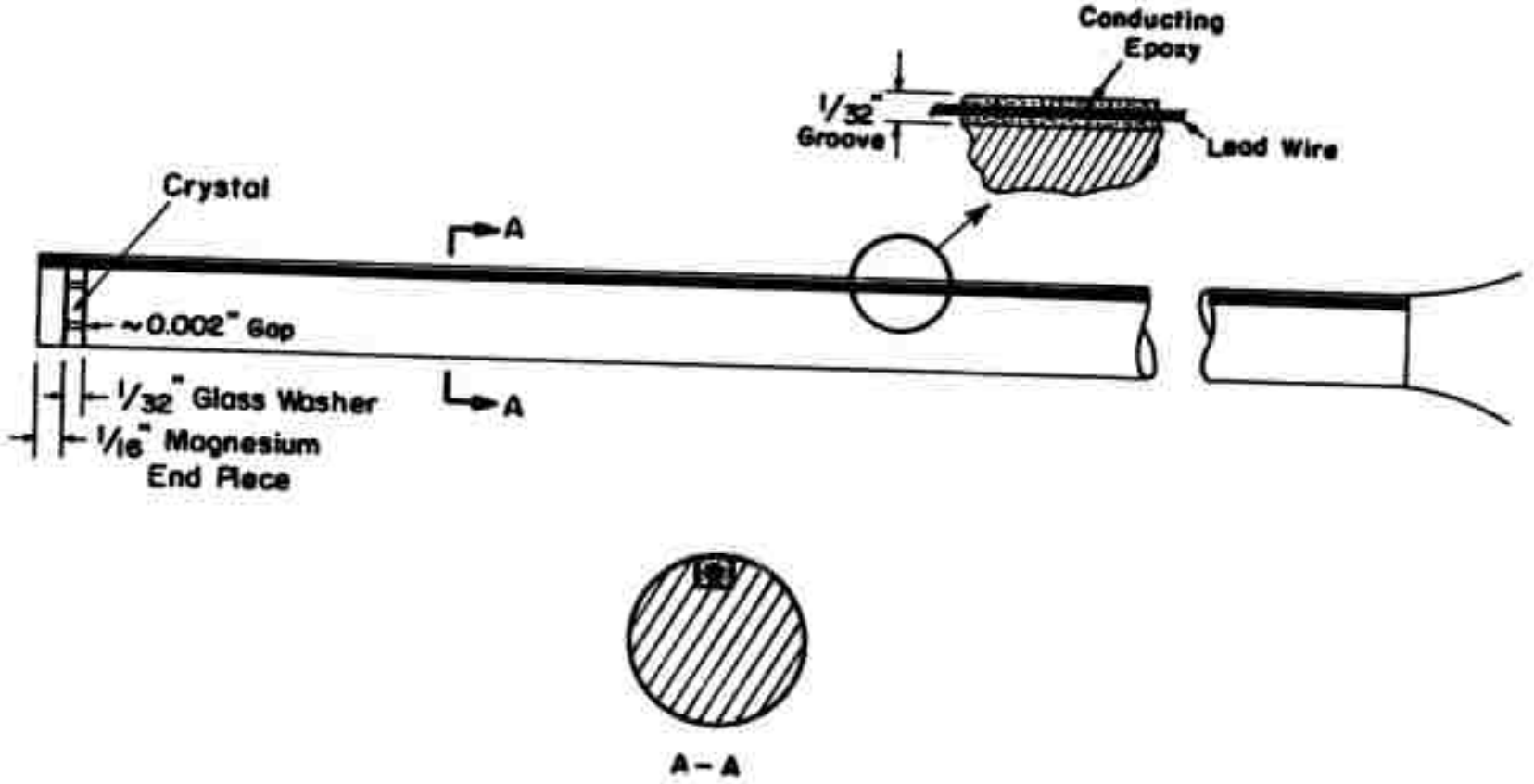
Conducting
Epoxy
1/32"
Groove
Lead Wire
Crystal
A
~0.002" Gap
1/32" Glass Washer
1/16" Magnesium
End Piece
A
A-A

Fig. 11

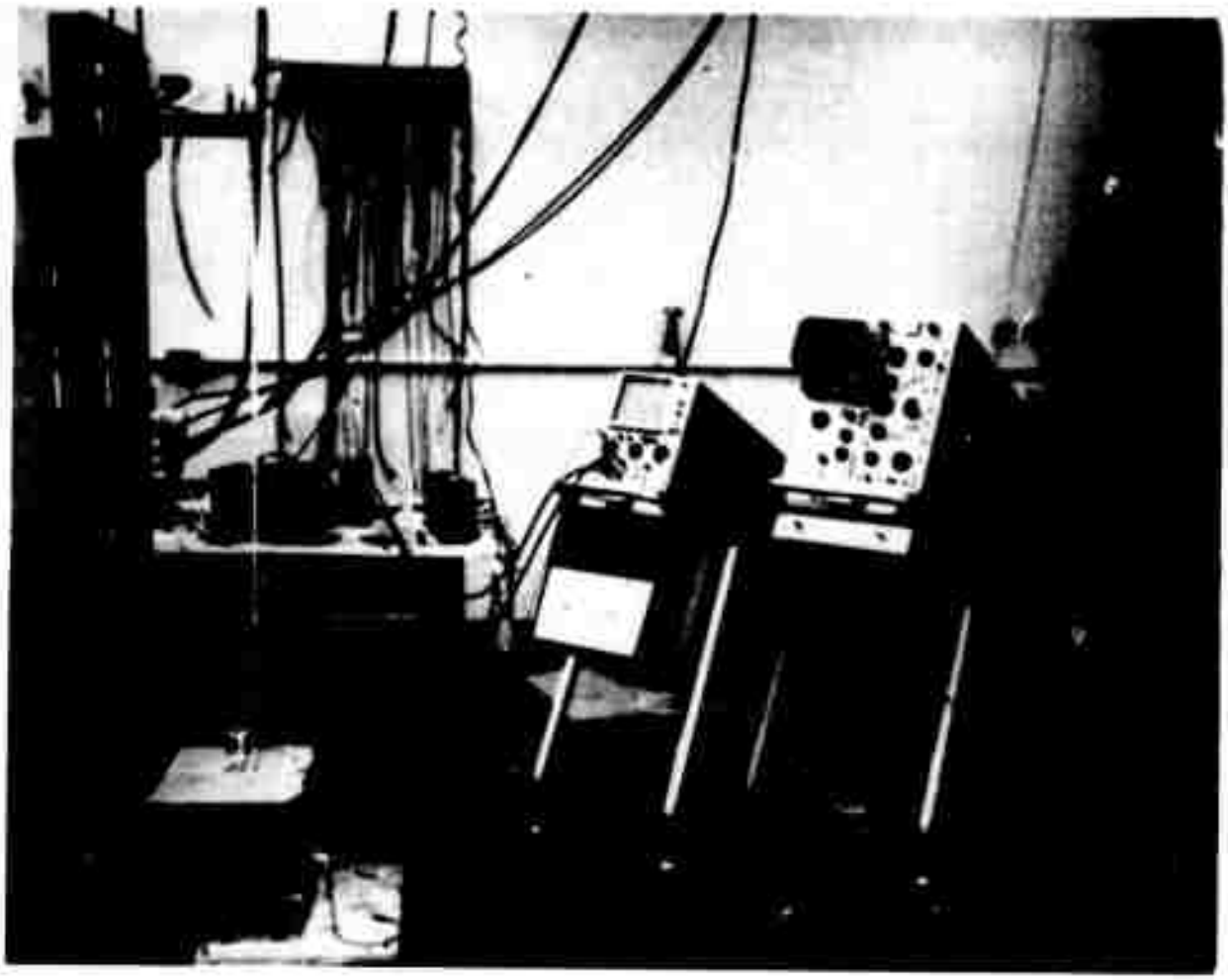

Fig. 12

20 μ sec/div

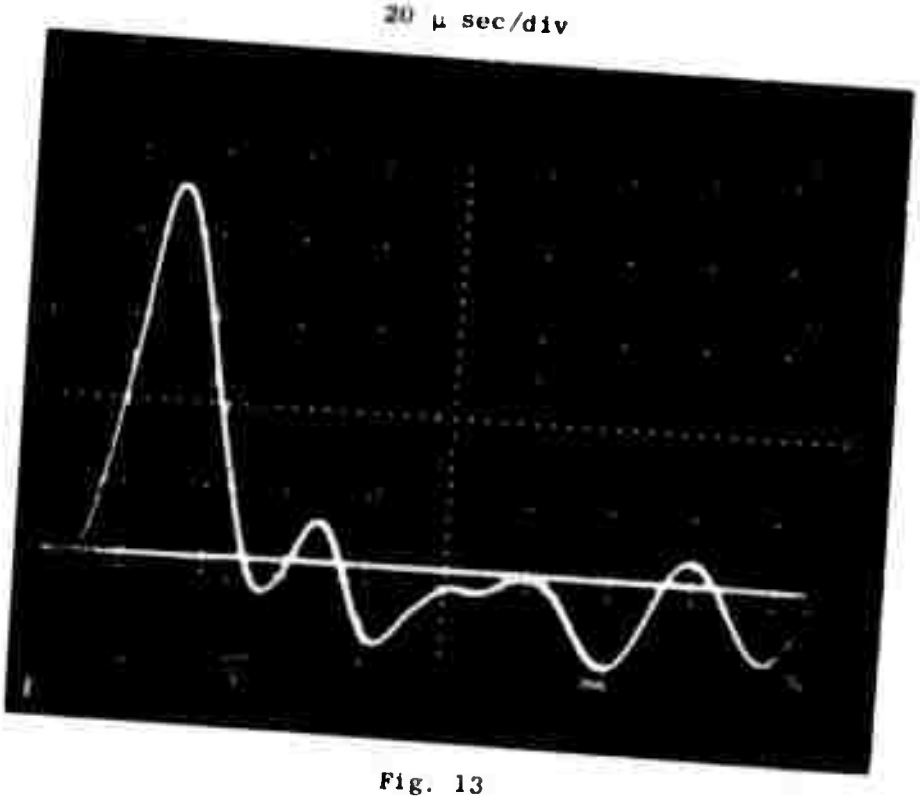

0.2 v/div

Fig. 13

50 μ sec/div

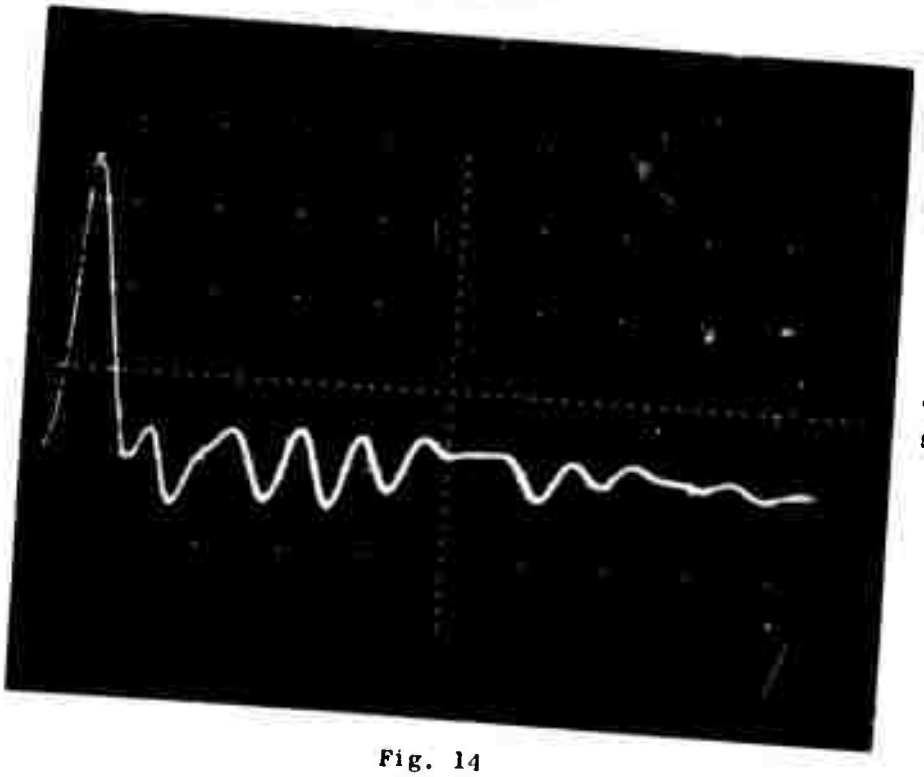

5v/div

Transducer sensitiivty: 10 ncb

Range: 2lb/volt

Fig. 14

Fig. 15

10 μ sec./div.

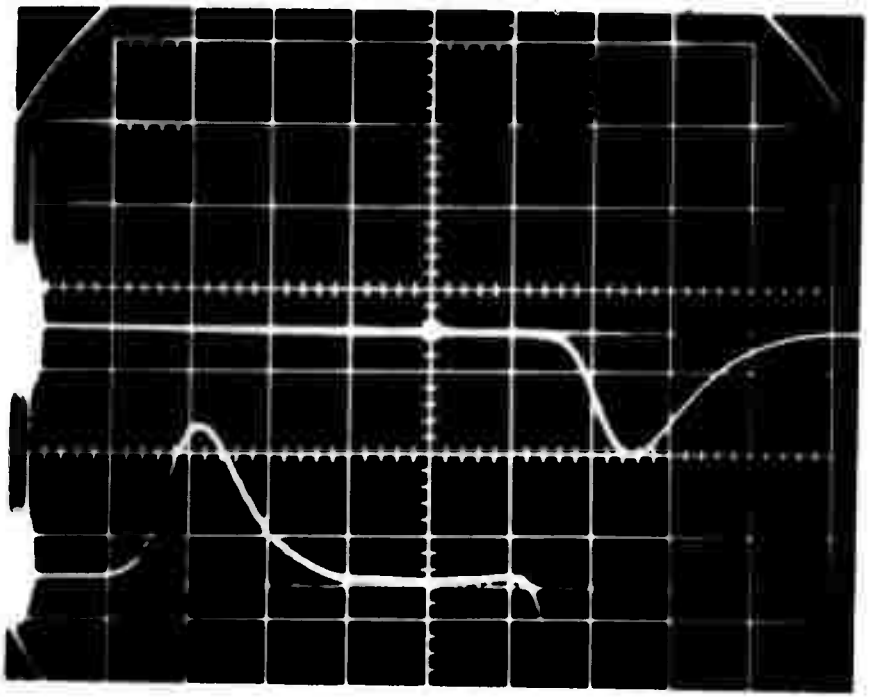

Crystal response
2v/div.

Strain gage response
2mv/div.

Fig. 16

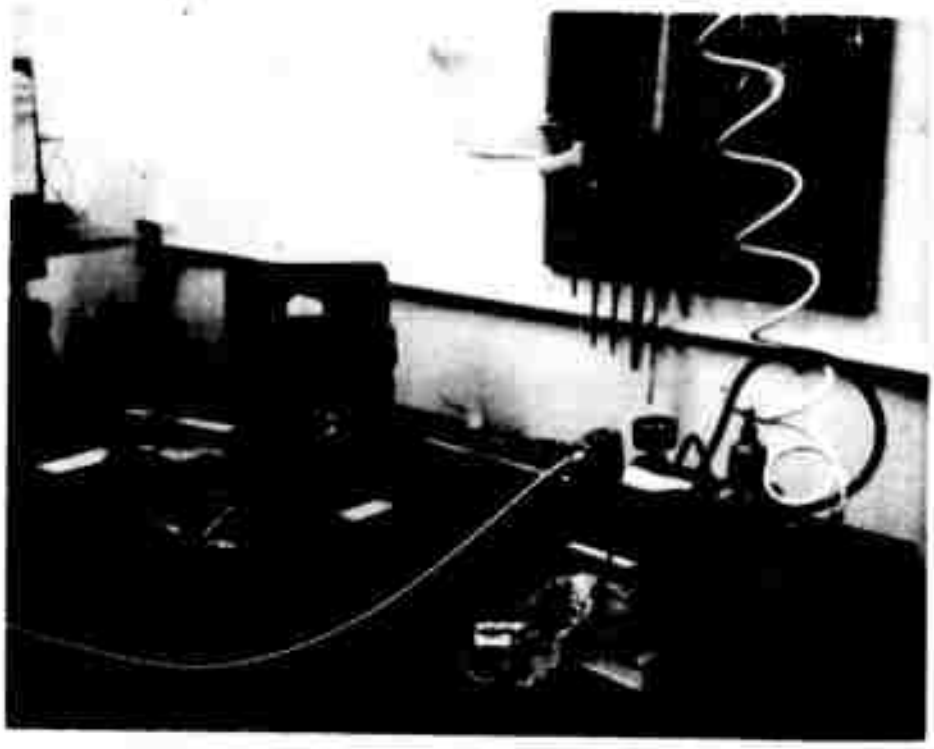

Fig. 17

10 μ sec./div.

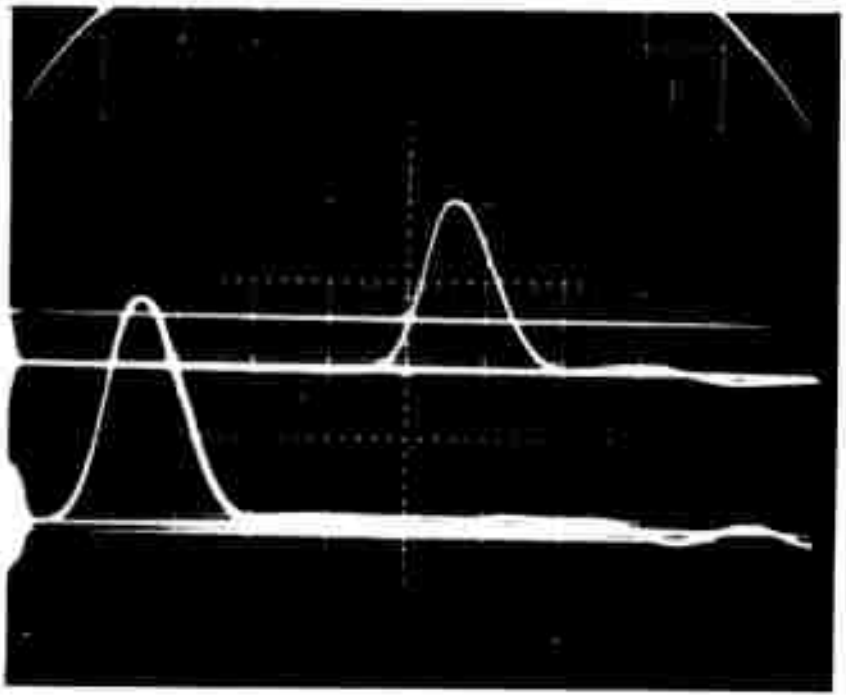

Crystal response
2v/div.

Strain gage response
2mv/div.

Fig. 18

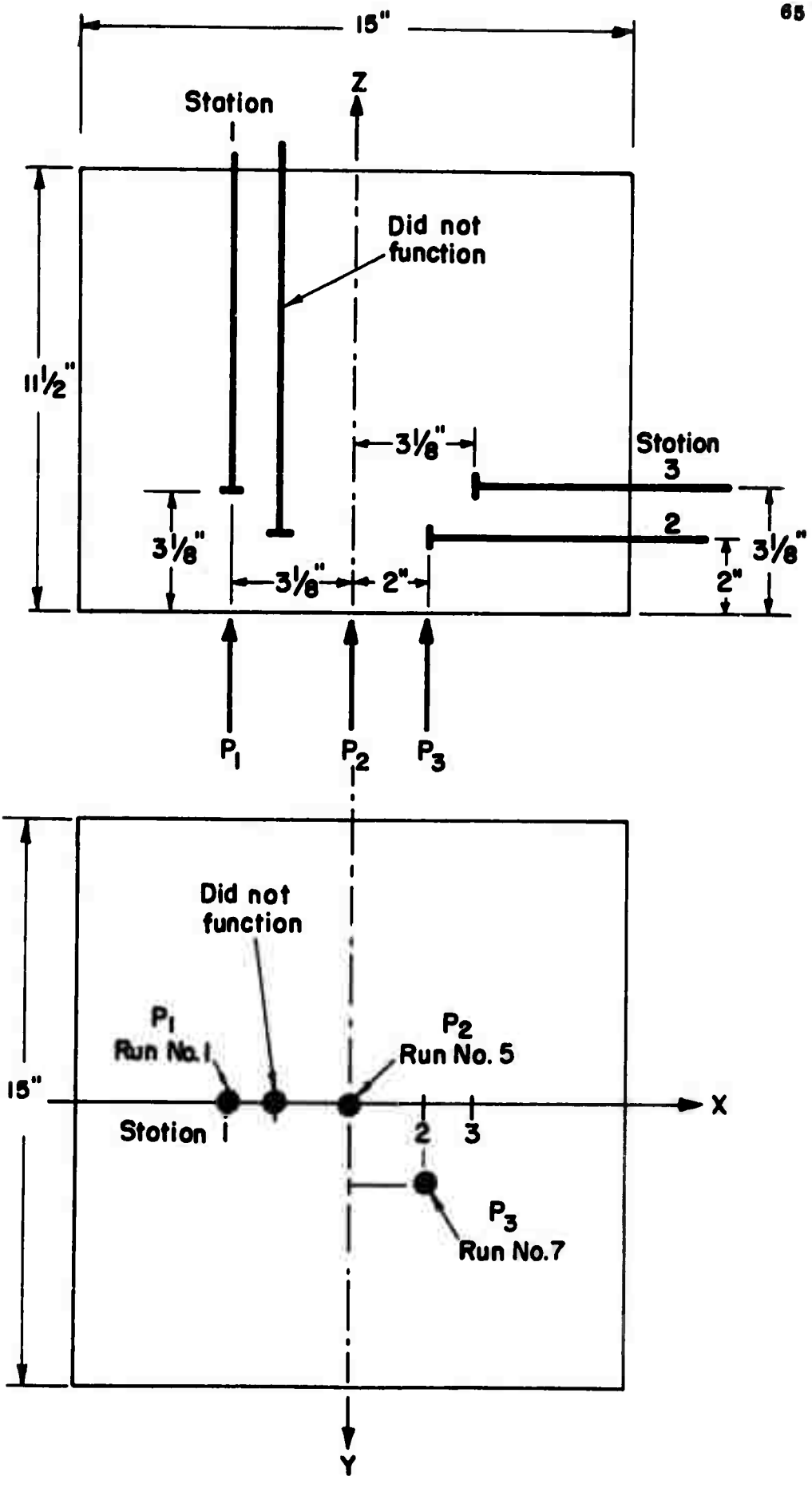
15"
Station 1
Z
Did not function
11½"
3⅛"
Station 3
2
3⅛"
3⅛"
3⅛"
2"
2"
P1
P2
P3
Did not function
P1
Run No. 1
P2
Run No. 5
15"
Station 1
2
3
X
P3
Run No. 7
Y

Fig. 19

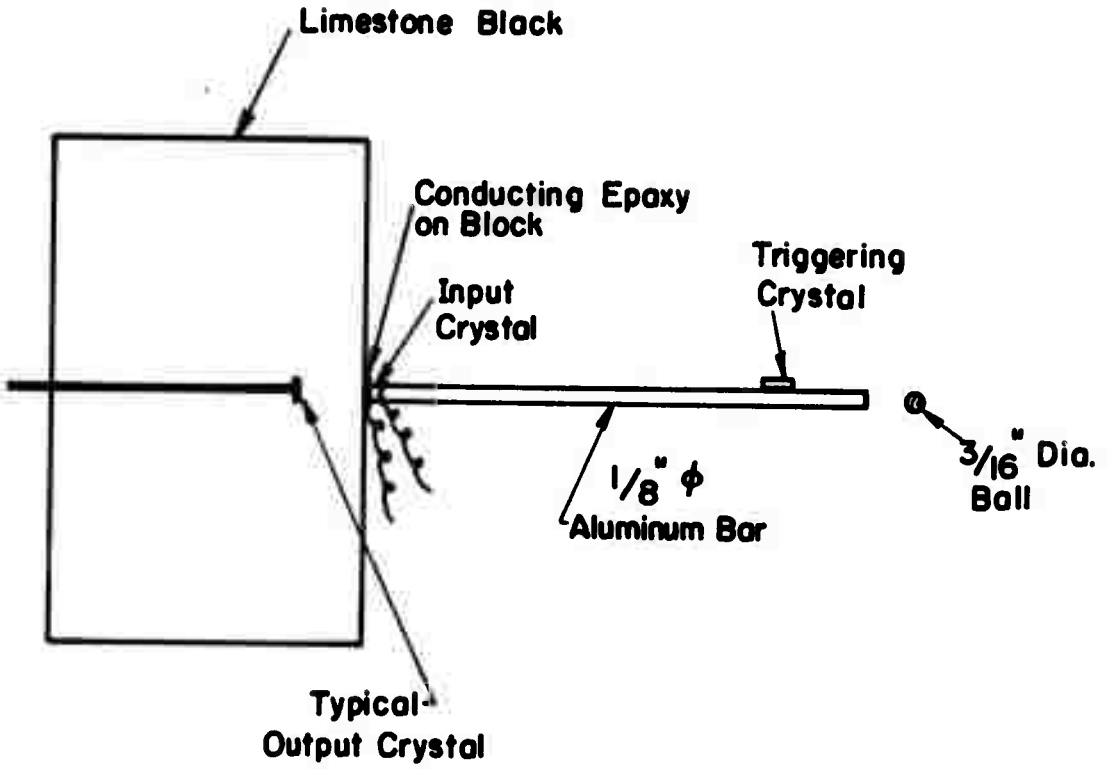
Limestone Block
Conducting Epoxy on Block
Input Crystal
Triggering Crystal
1/8" ϕ Aluminum Bar
3/16" Dia. Ball
Typical Output Crystal

Fig. 20

20 μ sec/div.

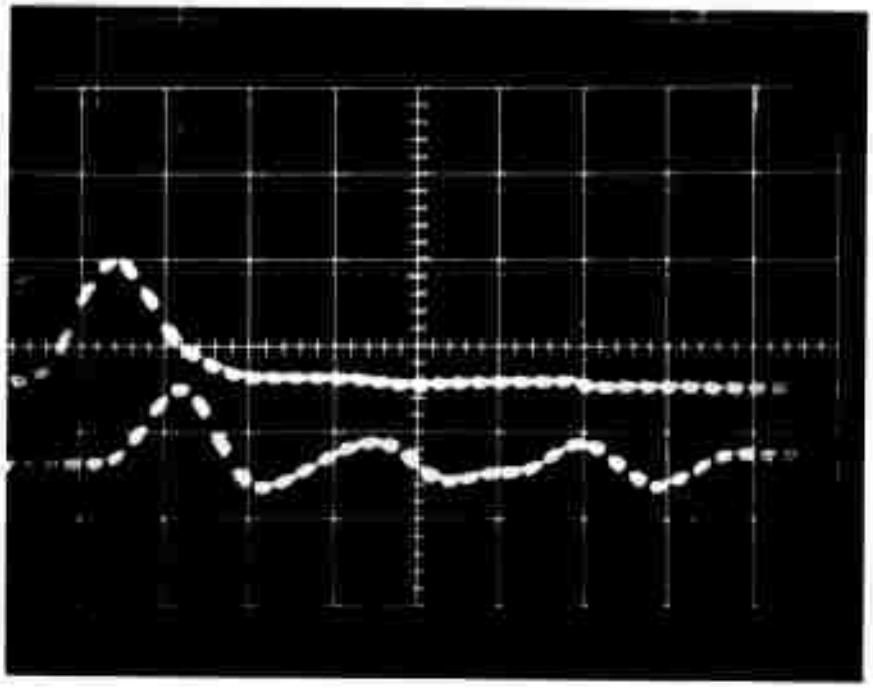

Run No. 1

x-cut quartz
Input crystal
response by
charge amplification

0.5 v/div.

Output at Station No. 1
by charge amplification

0.5 v/div.

Fig. 21(a)

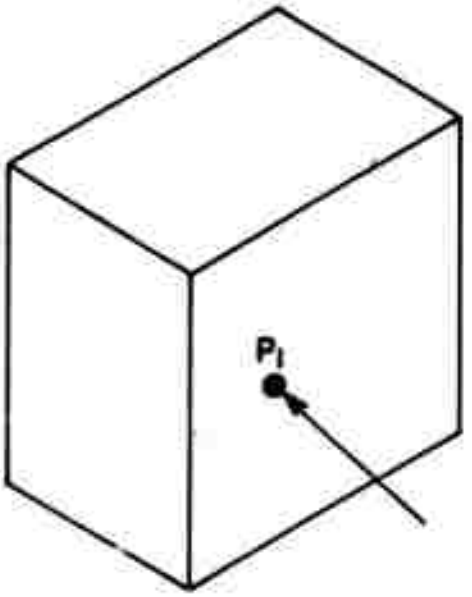

Run No. 1

Fig. 21(b)

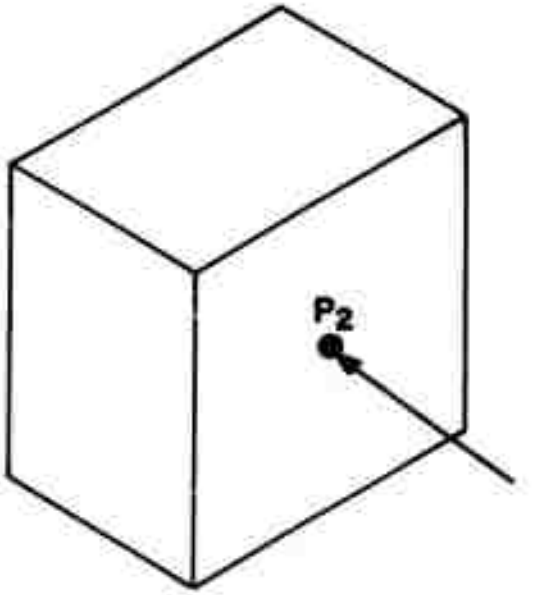

Run No. 5

Fig. 22

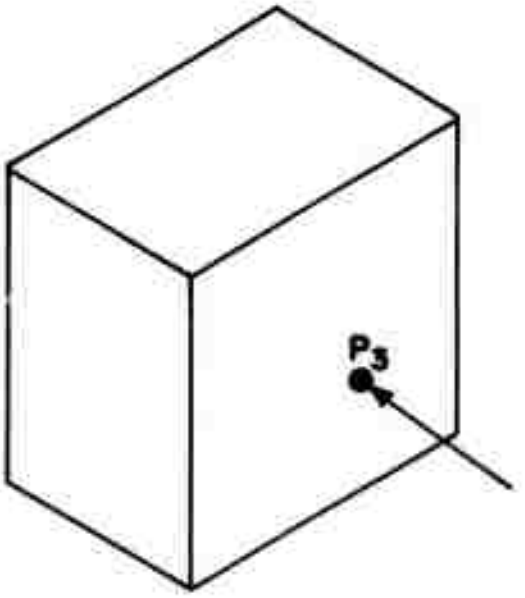

Run No. 7

(See Fig. 19)

Fig. 23

20 μ sec./div.

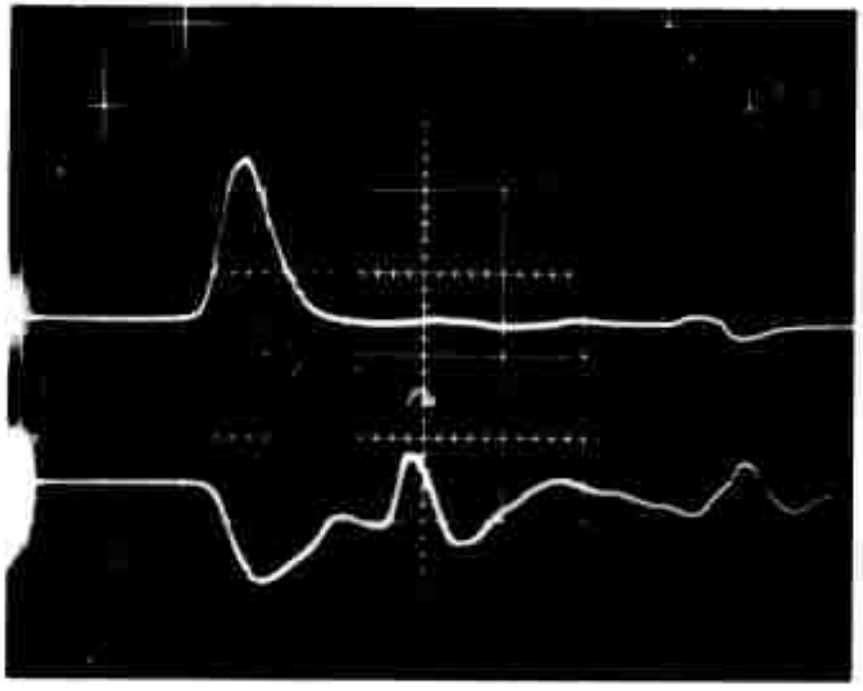

Run No. 5

PZT-5a Input
Crystal response
5v/div. ; 100 x

Output crystal
response at
Station No. 2
0.2v/div.

Fig. 24

20 μ sec./div.

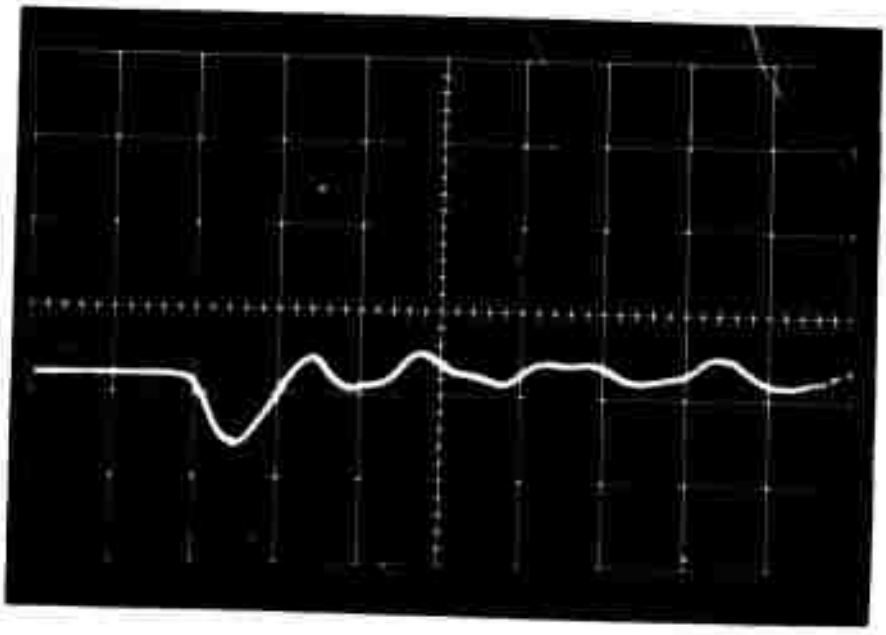

Run No. 5

Output Crystal response at Station No. 1 0.2v/div.

Fig. 25

20 μ sec./div.

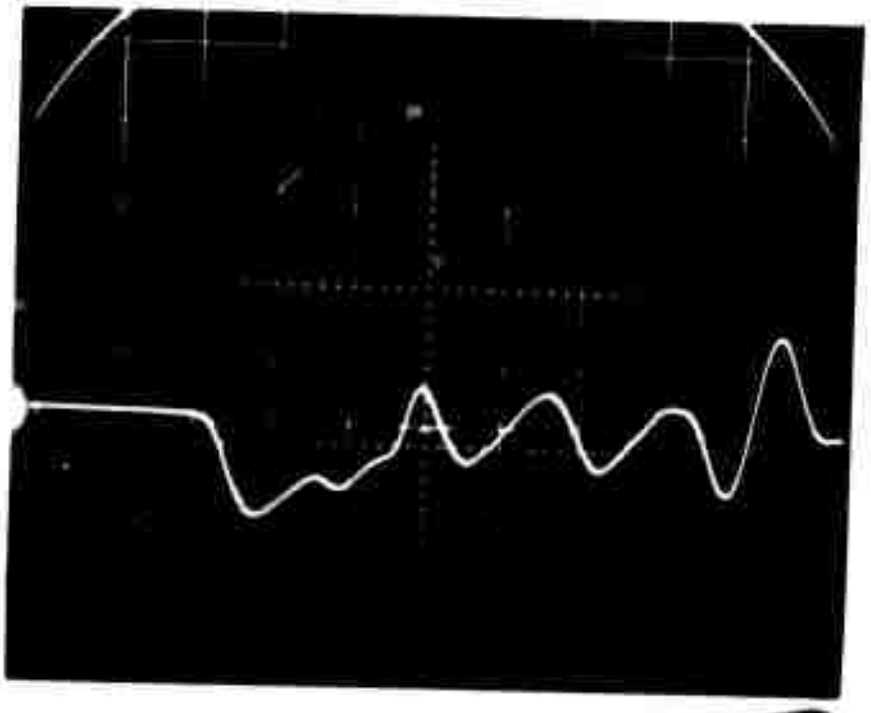

Run No. 5

Output Crystal response at Station No. 3 0.1v/div.

Fig. 26

20 μ sec./div.

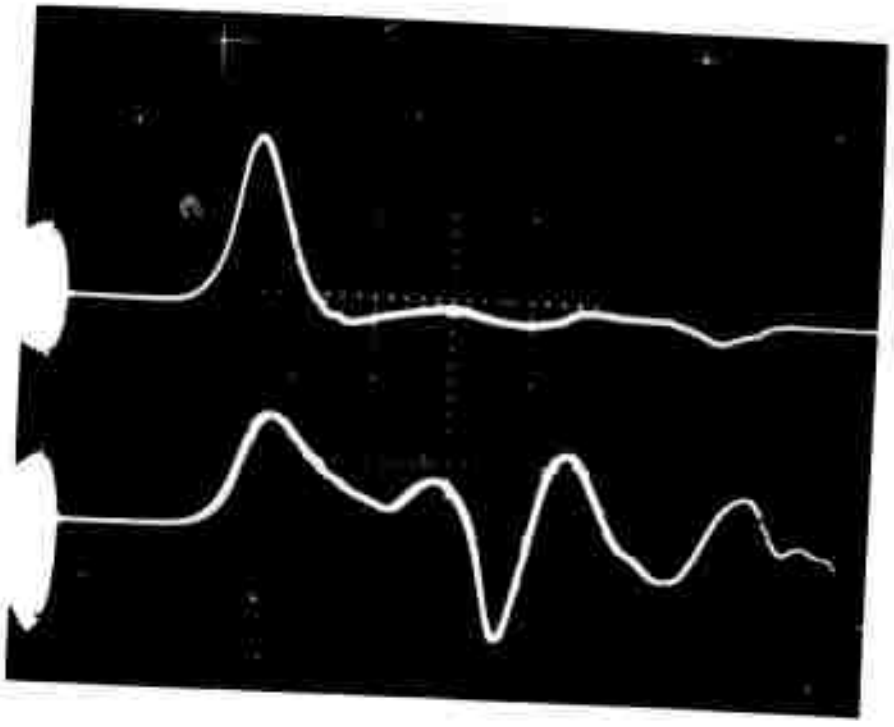

Run No. 7
PZT-5a
Input crystal response
5v/div.; 100X

Output crystal response at Station No. 2
0.1v/div.

Fig. 27

20 μ sec./div.

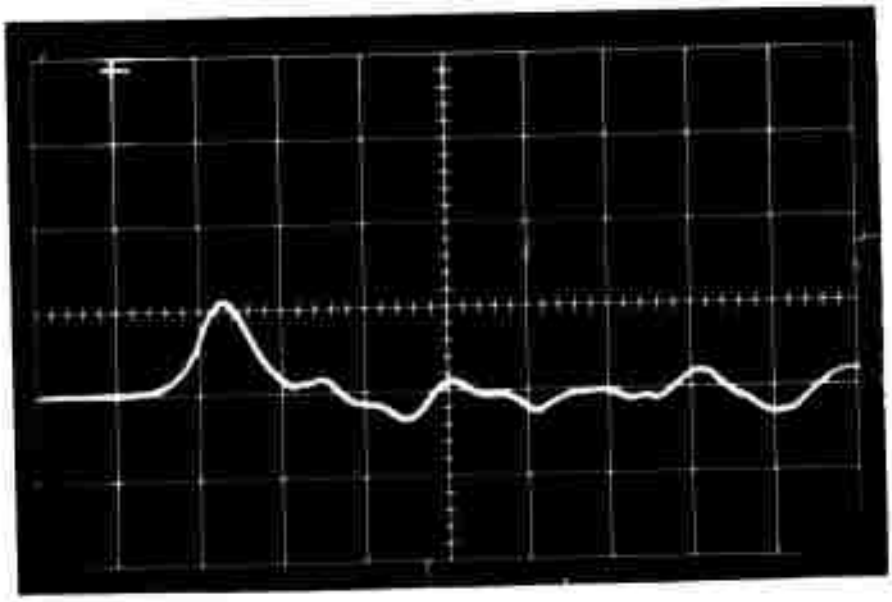

Run No. 7

Output crystal response at Station No. 1 0.1v/div.

Fig. 28

20 μ sec./div.

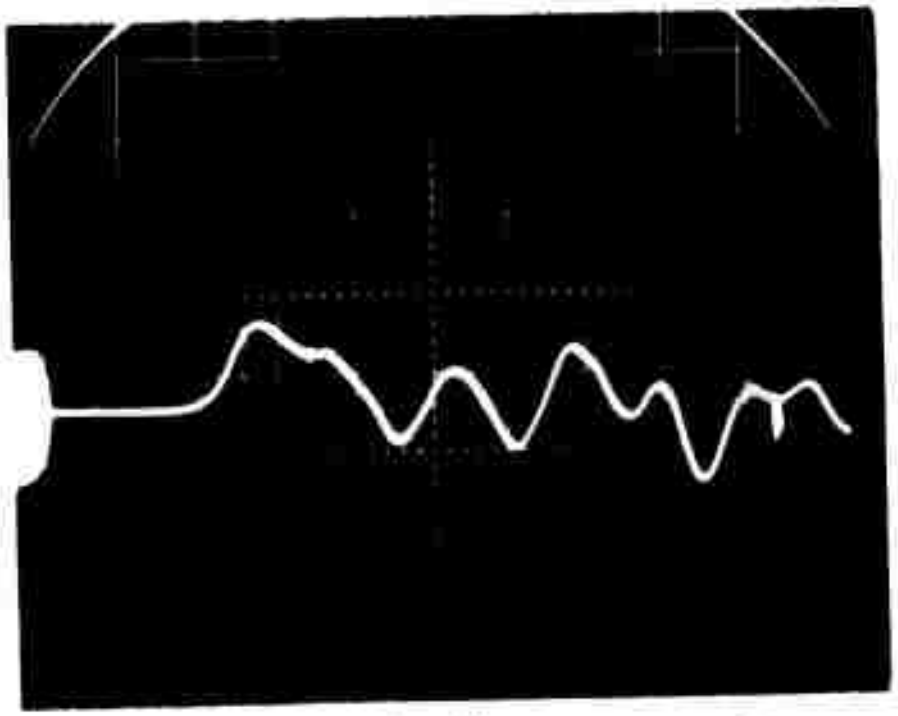

Run No. 7

Output crystal response at Station No. 3 0.1v/div.

Fig. 29

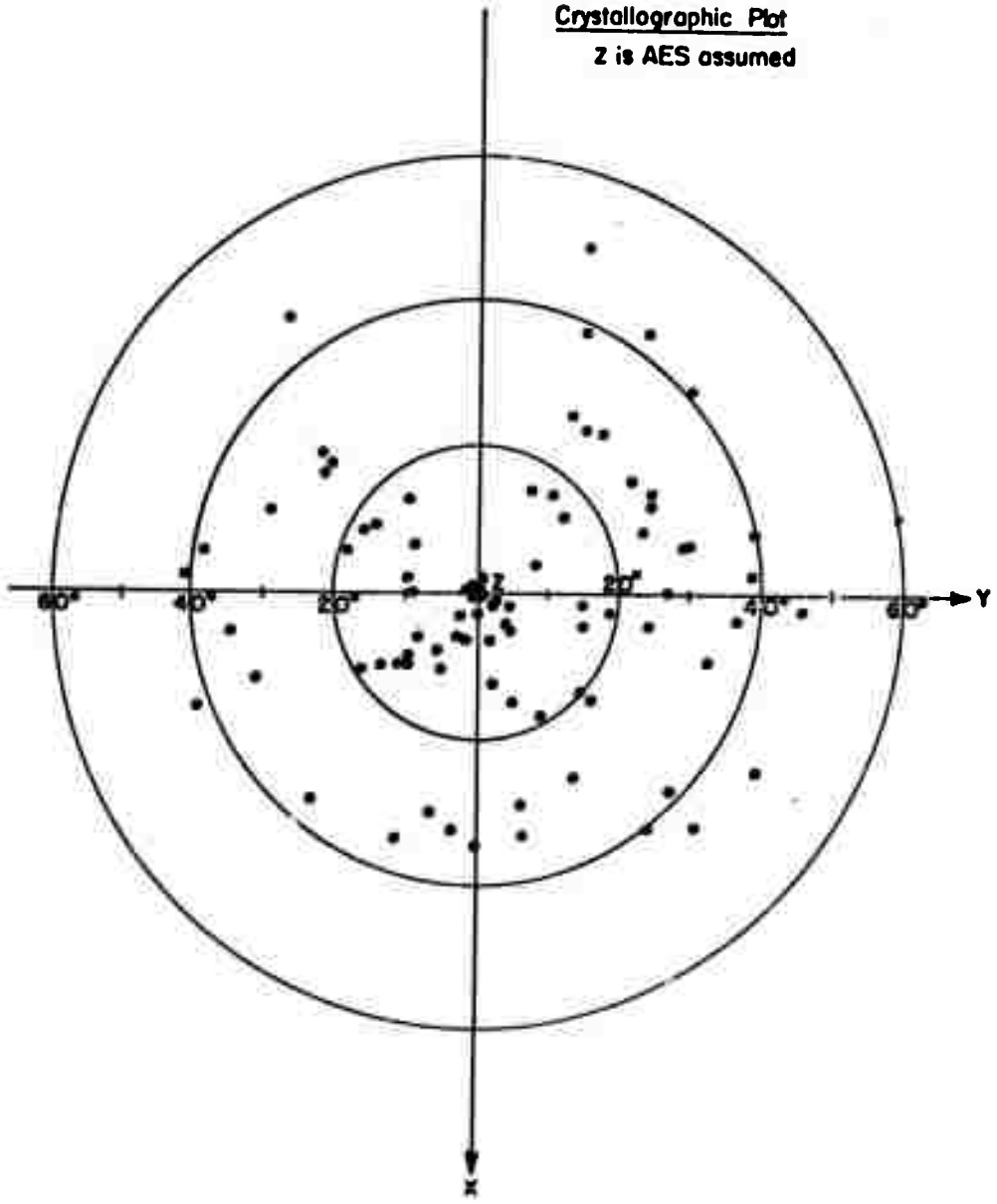

Fig. 30

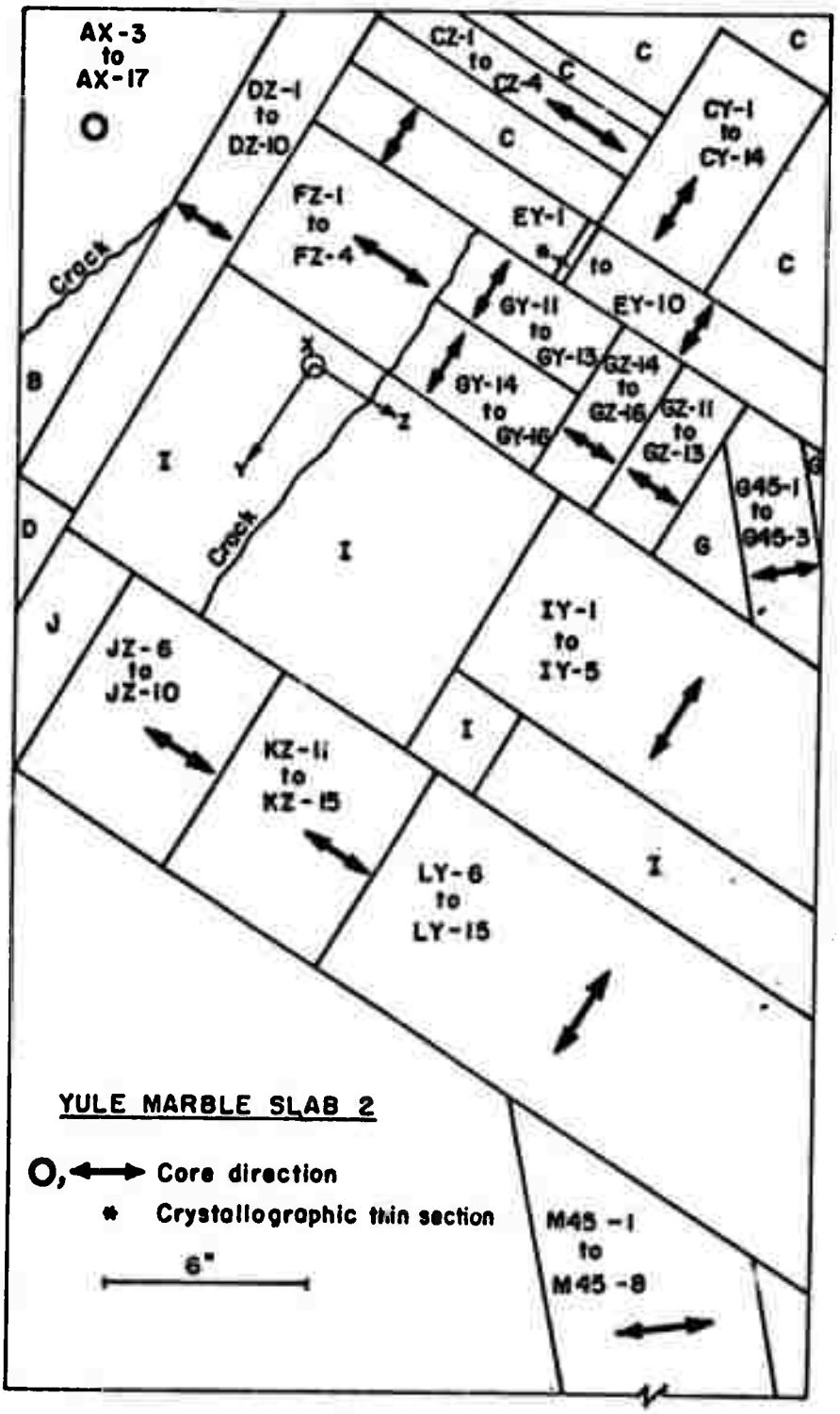
AX-3
to
AX-17
DZ-1
to
DZ-10
CZ-1
to
CZ-4
C
C
C
C
CY-1
to
CY-14
FZ-1
to
FZ-4
EY-1
to
EY-10
GY-11
to
GY-13
GY-14
to
GY-16
GZ-14
to
GZ-16
GZ-11
to
GZ-13
G45-1
to
G45-3
Crack
B
I
D
J
JZ-6
to
JZ-10
KZ-11
to
KZ-15
IY-1
to
IY-5
LY-6
to
LY-15
M45-1
to
M45-8
YULE MARBLE SLAB 2
Core direction
Crystallographic thin section
6"

Fig. 31

Fig. 32a

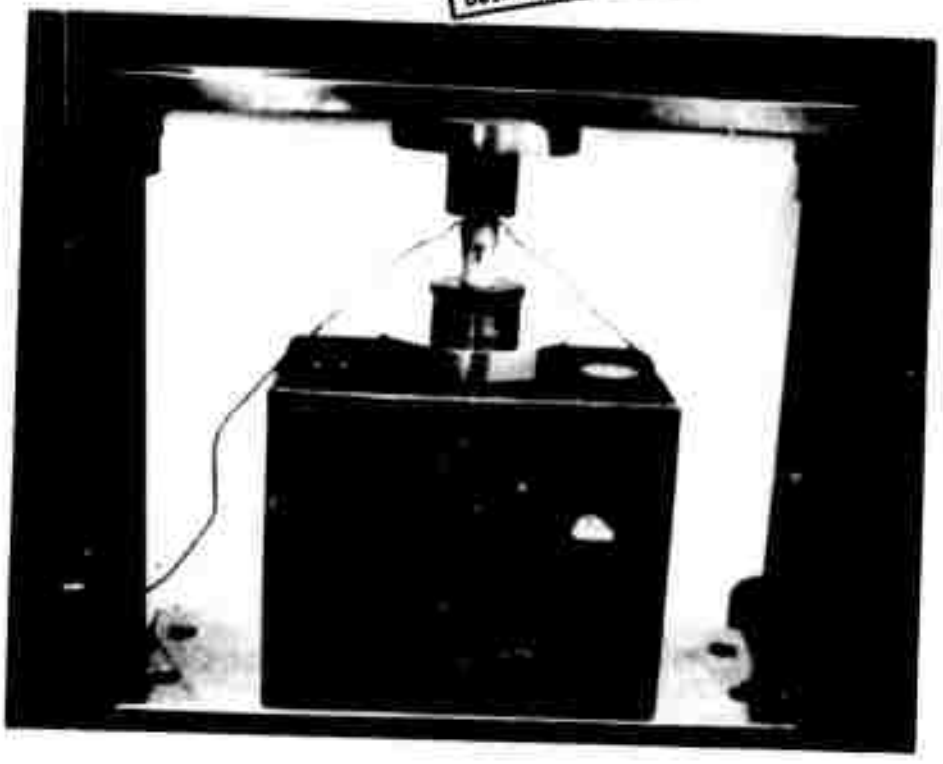

Fig. 32b

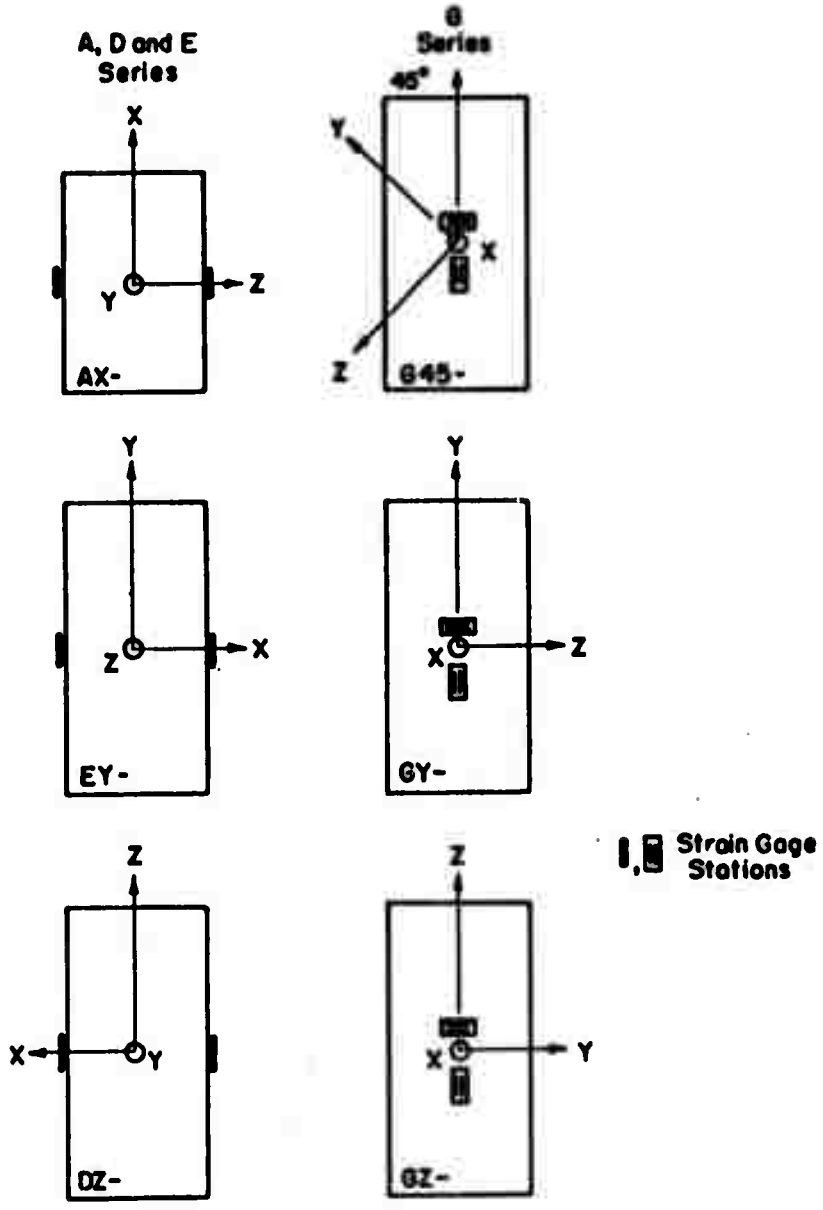

Z is Axis of Elastic Symmetry

Fig. 33

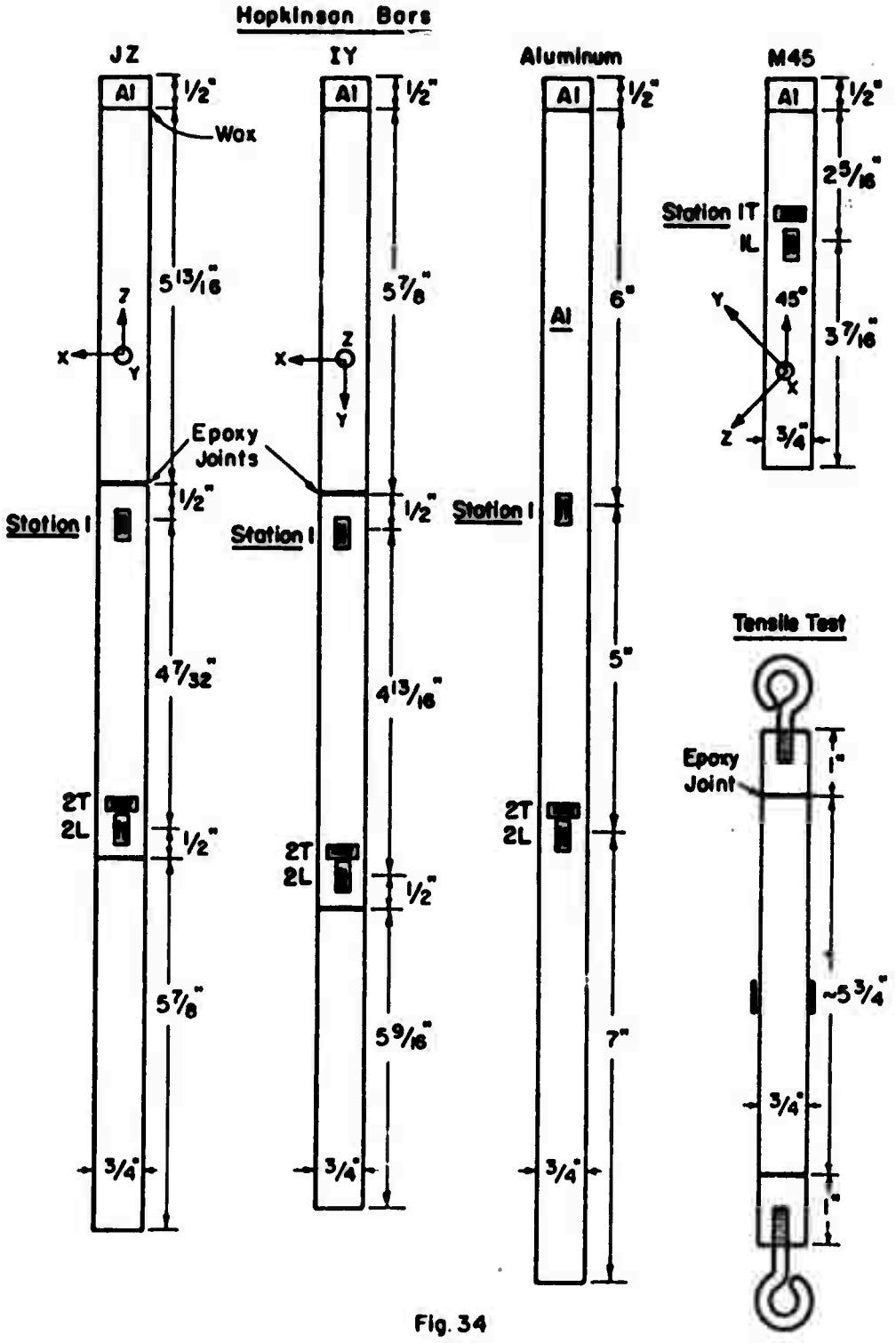
Hopkinson Bars
JZ
IY
Aluminum
M45
Al
1/2"
Wax
5 13/16"
Z
X
Y
Epoxy Joints
Station I
1/2"
4 7/32"
2T
2L
5 7/8"
3/4"
5 7/8"
4 13/16"
5 9/16"
6"
5"
7"
Station IT
IL
45°
2 5/16"
3 7/16"
3/4"
Tensile Test
Epoxy Joint
1"
~5 3/4"

Fig. 34

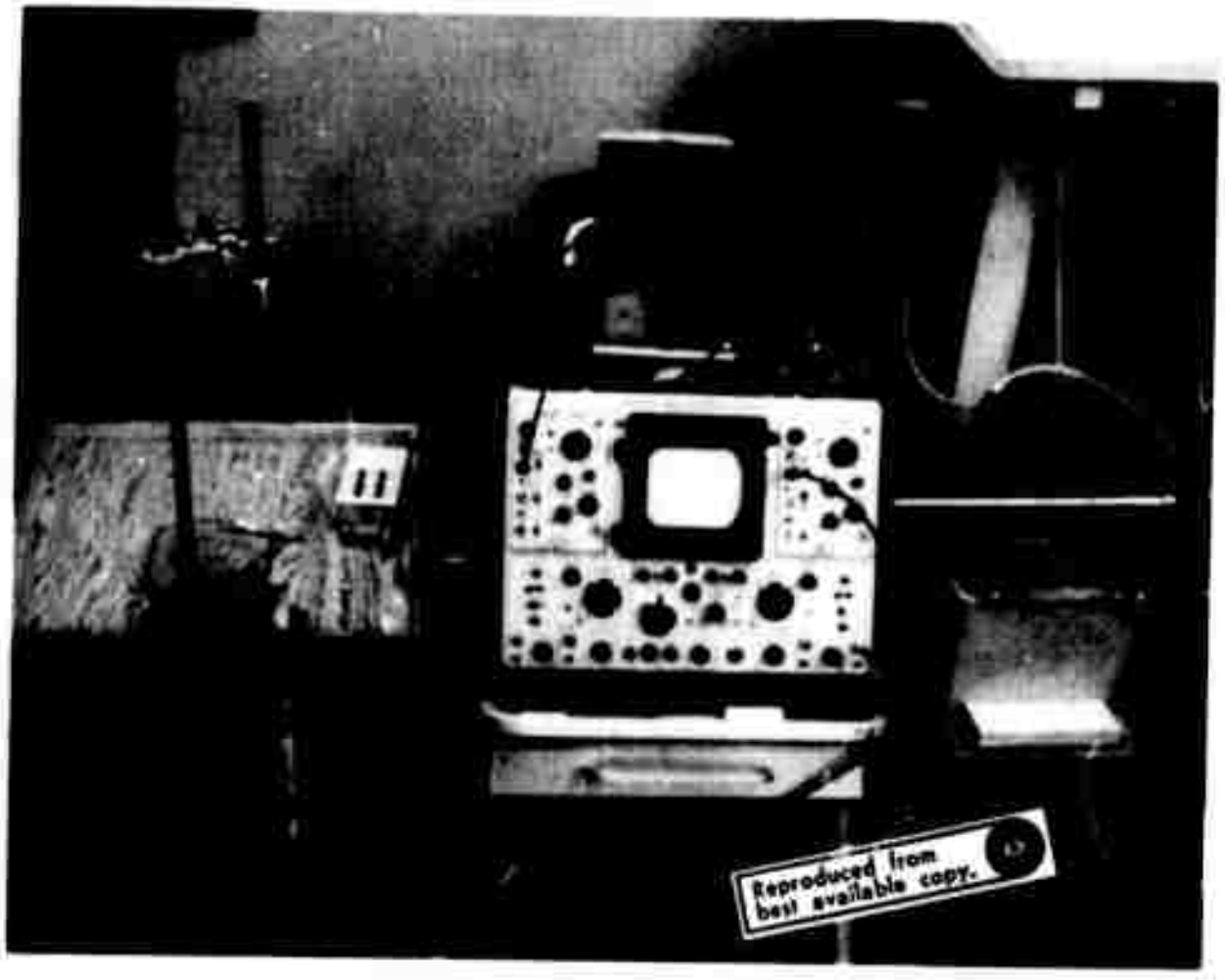

Fig. 35

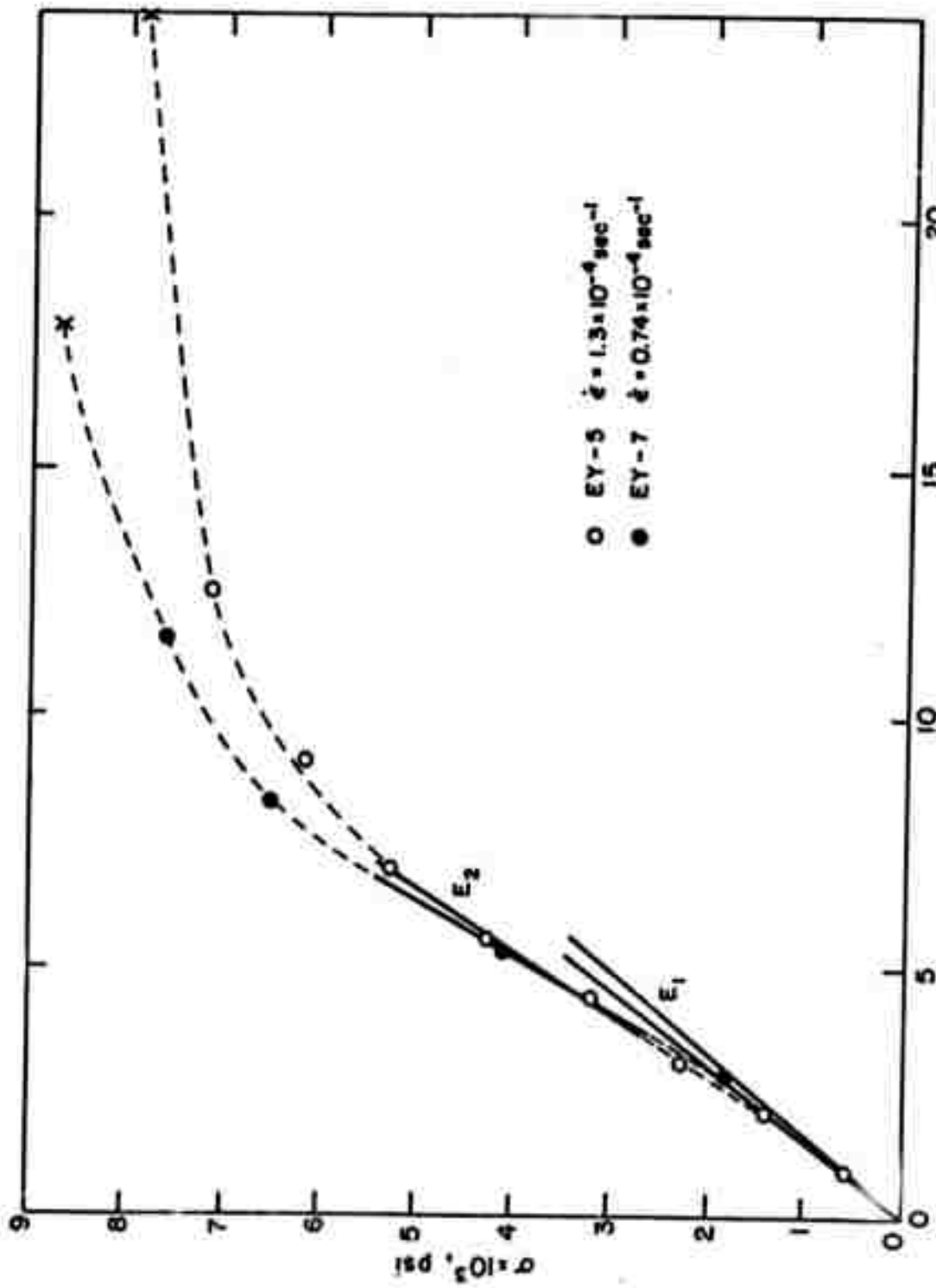

Fig. 36

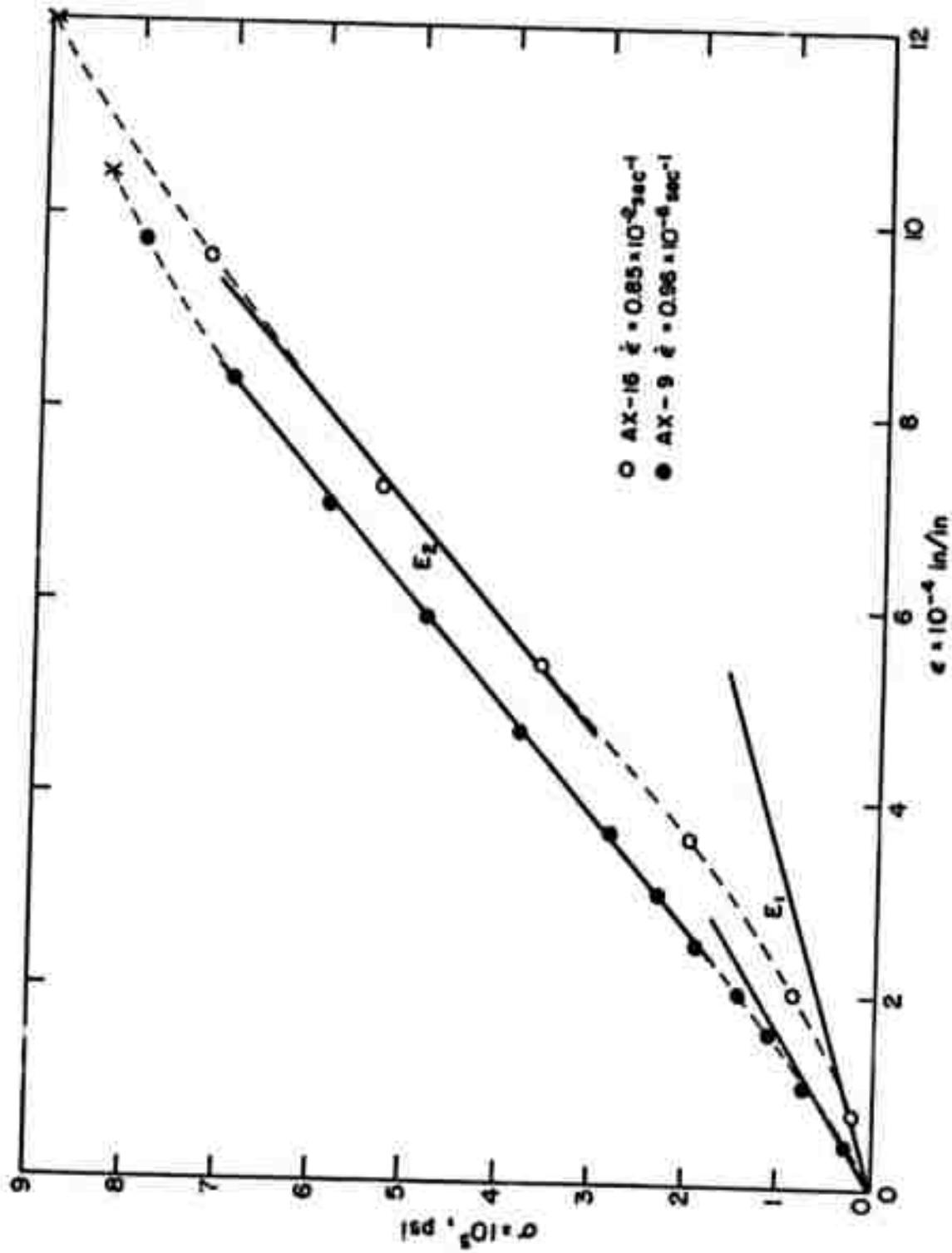
AX-16 $\dot{\epsilon}$ = 0.85 x 10^{-2} sec^{-1}
AX-9 $\dot{\epsilon}$ = 0.96 x 10^{-4} sec^{-1}
E_2
E_1
$\sigma \times 10^3$, psi
$\epsilon \times 10^{-4}$ in/in

Fig. 37

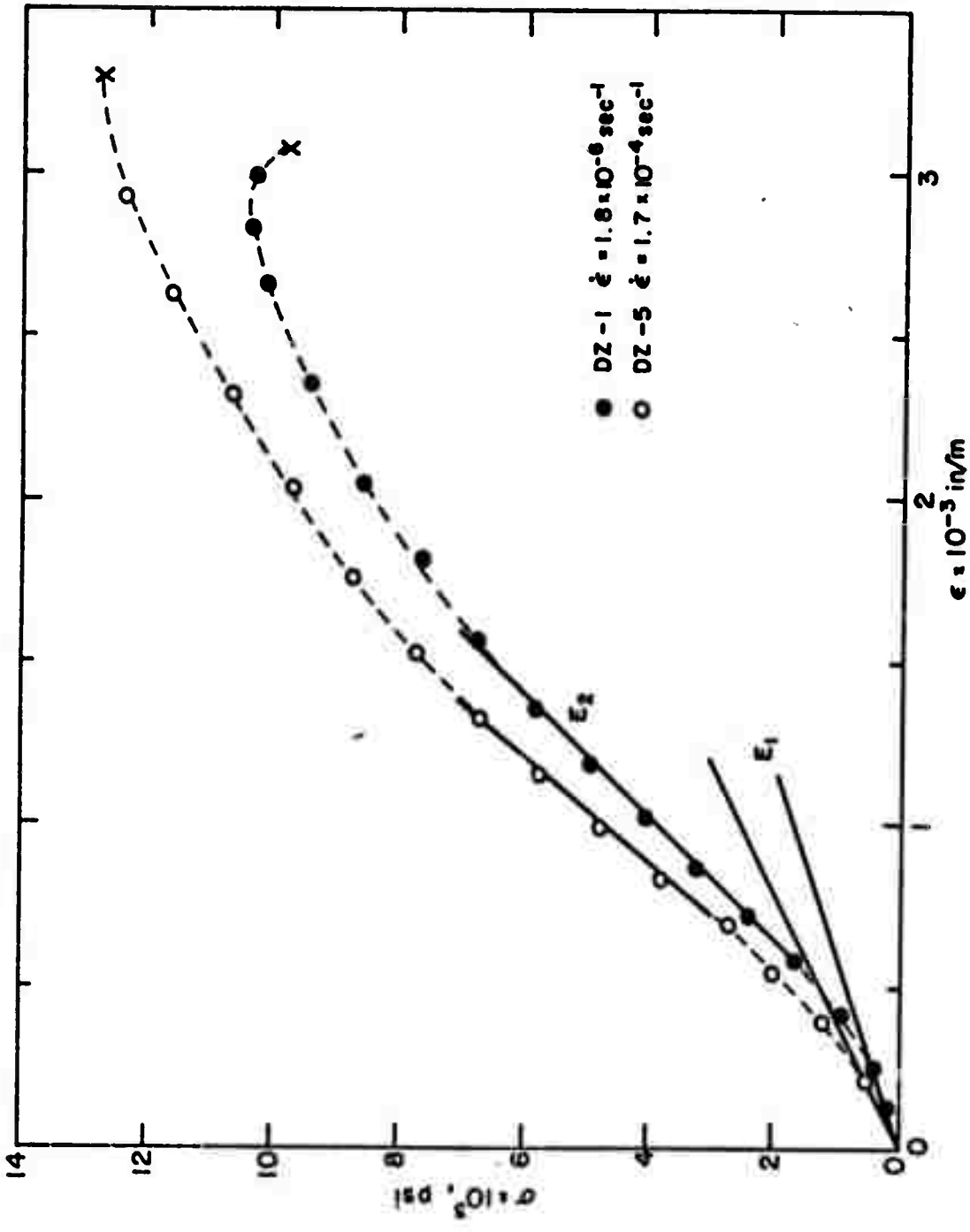
DZ-1 $\dot{\epsilon}$ = 1.8×10⁻⁶ sec⁻¹
DZ-5 $\dot{\epsilon}$ = 1.7×10⁻⁴ sec⁻¹
E₂
E₁
σ × 10³, psi
ε × 10⁻³ in/in
0
2
4
6
8
10
12
14
1
3

Fig. 38

Figure 39

TABLE OF E_1 & E_2 vs. ϵ & DIRECTION

SPECIMEN I.D.	$\dot{\epsilon}$ sec^{-1}	E_1 $x10^6$ psi	E_2 $x10^6$ psi
AX-8	$.9 \times 10^{-6}$	5.5	8.9
AX-9	1.0×10^{-6}	6.6	9.1
AX-10	1.0×10^{-5}	6.4	8.9
AX-11	$.9 \times 10^{-5}$	3.8	9.3
AX-12	1.0×10^{-4}	5.0	9.3
AX-13	1.0×10^{-4}	6.6	9.1
AX-14	1.2×10^{-3}	-	-
AX-15	1.2×10^{-3}	-	-
AX-16	$.9 \times 10^{-2}$	6.9	9.0
AX-17	$.9 \times 10^{-2}$	4.4	8.1
EY-1	1.1×10^{-6}	6.4	8.4
EY-2	1.1×10^{-6}	8.8	8.8
EY-3	1.1×10^{-5}	6.3	8.3
EY-4	1.1×10^{-5}	6.1	8.4
EY-5	1.3×10^{-4}	5.8	8.0
EY-6	1.2×10^{-4}	6.3	8.4
EY-7	$.7 \times 10^{-4}$	6.5	8.5
EY-8	1.2×10^{-3}	-	-
EY-9	1.0×10^{-2}	9.6	6.4
EY-10	1.3×10^{-2}	6.2	7.5

SPECIMEN I.D.	$\dot{\epsilon}$ sec^{-1}	E_1 $x10^6$ nsi	E_2 $x10^6$ nsi
DZ-1	$1.8x10^{-6}$	1.7	5.3
DZ-2	$2.0x10^{-6}$	2.9	6.2
DZ-3	$1.6x10^{-6}$	2.8	6.2
DZ-4	$1.8x10^{-5}$	3.0	6.3
DZ-5	$1.7x10^{-4}$	2.4	6.2
DZ-6	$2.0x10^{-4}$	1.9	5.7
DZ-7	-	-	-
DZ-8	$5.7x10^{-3}$	2.9	5.0
DZ-9	-	-	-
DZ-10	$5.5x10^{-3}$	2.4	5.2
X ave	-	5.6	8.9
Y ave	-	6.6	8.1
Z ave	-	2.6	5.8

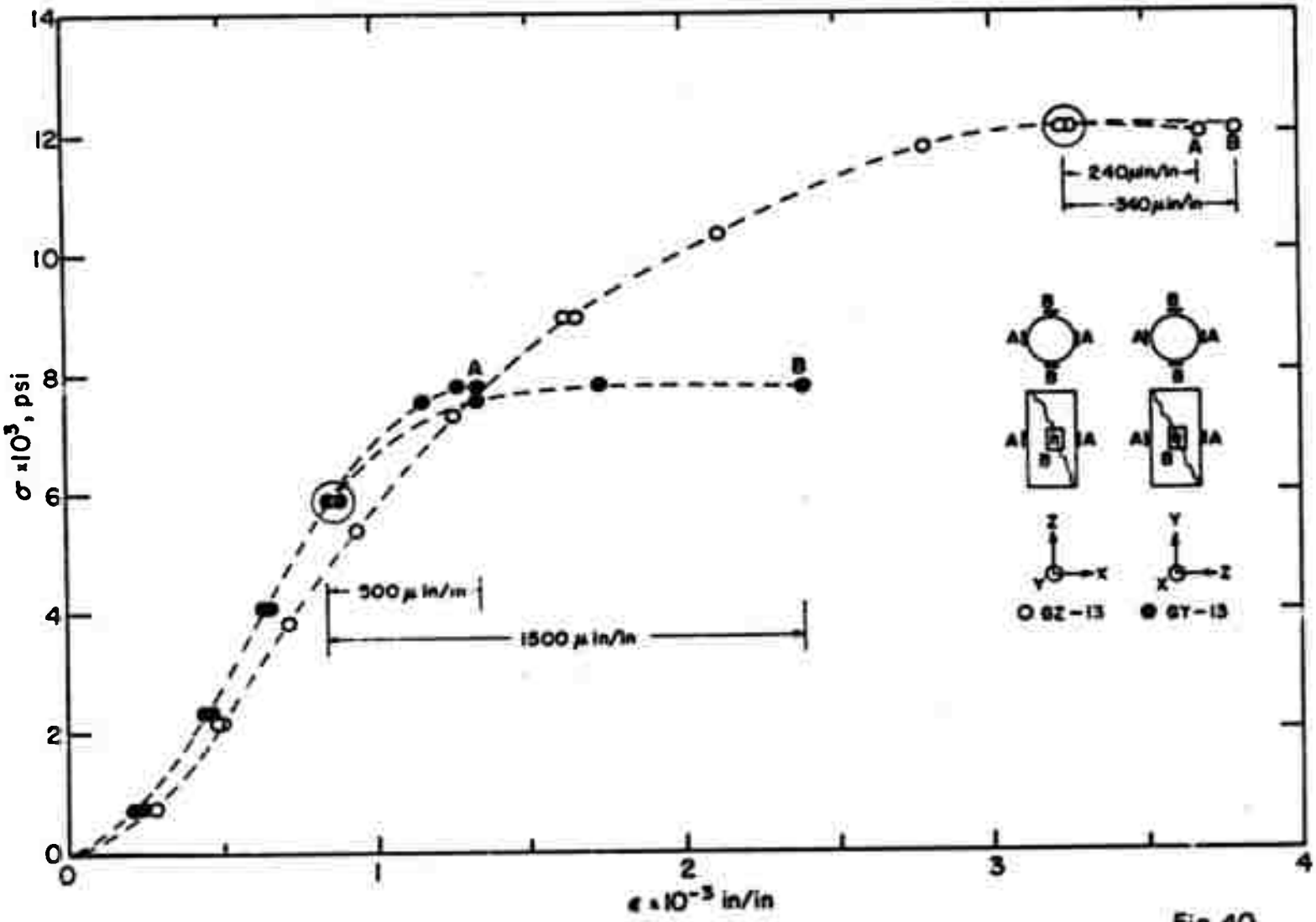
σ x10³, psi
ε x10⁻³ in/in
240μin/in
340μin/in
500 μ in/in
1500 μ in/in
A
B
O 6Z-13
● 6Y-13

Fig. 40

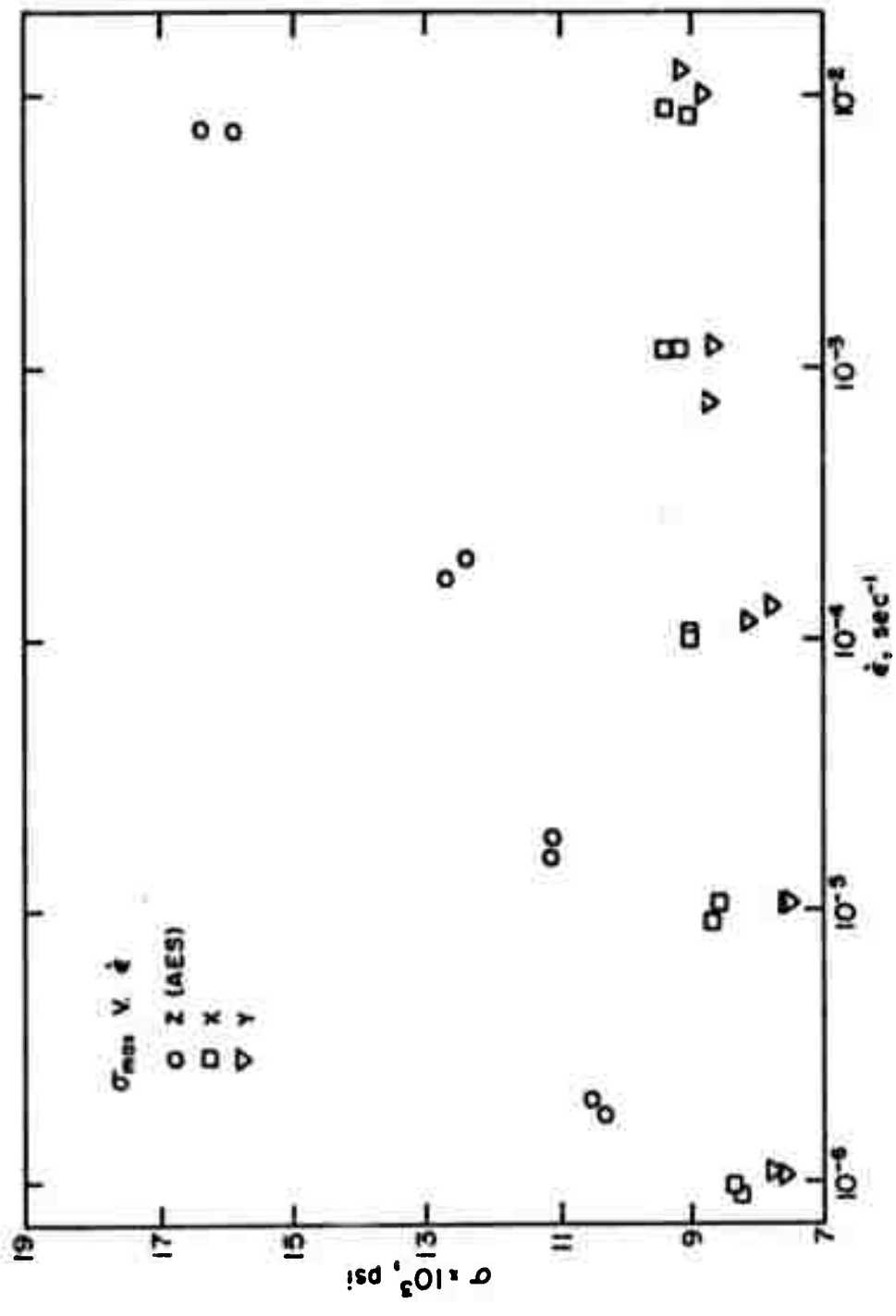
σ_{max} vs. $\dot{\epsilon}$
z (AES)
x
y
$\sigma \times 10^3$, psi
$\dot{\epsilon}$, sec^{-1}
19
17
15
13
11
9
7
10^{-6}
10^{-5}
10^{-4}
10^{-3}
10^{-2}

Fig. 41

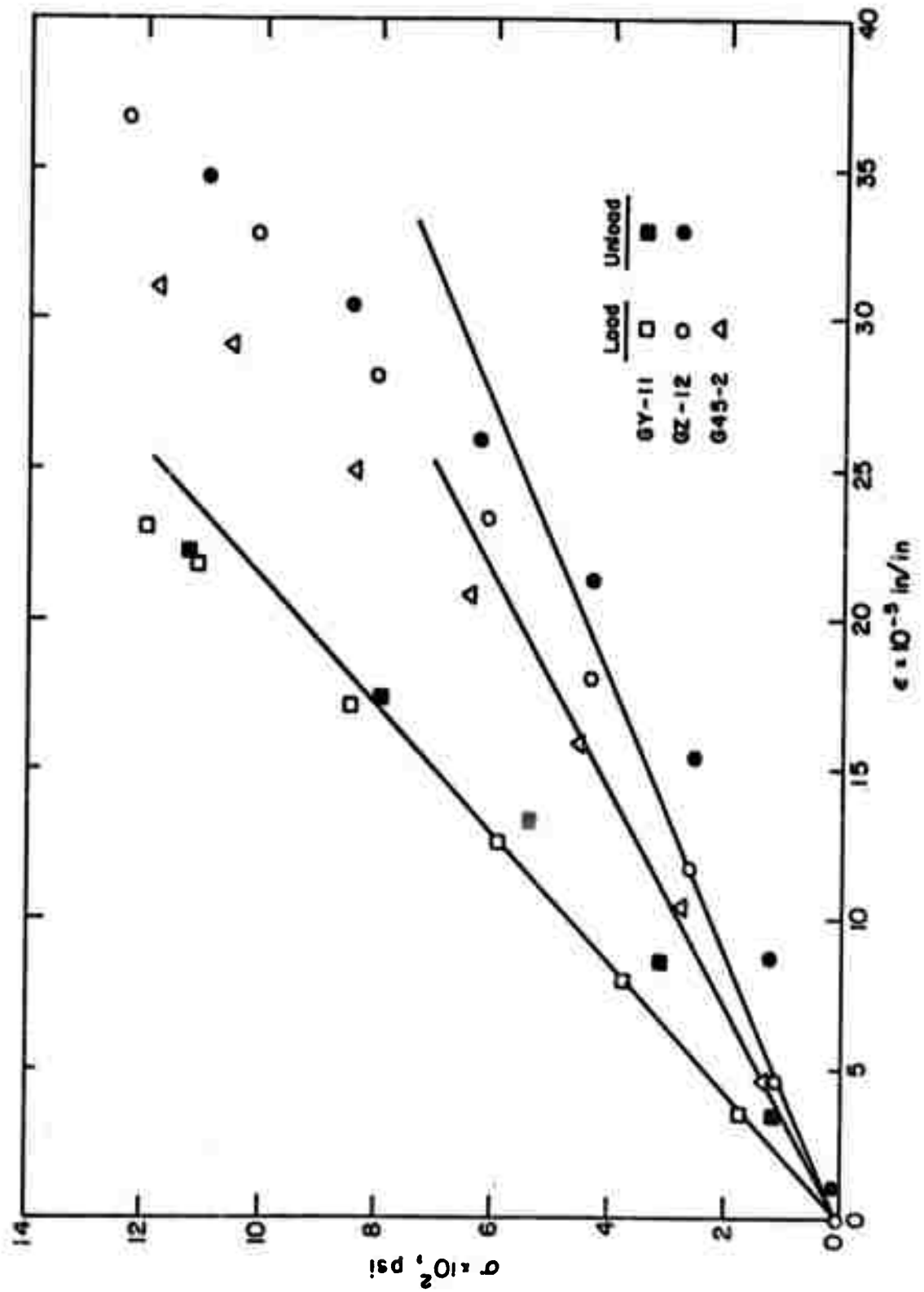
σ ×10², psi
ε ×10⁻³ in/in
Load
Unload
GY-11
GZ-12
G45-2
0
2
4
6
8
10
12
14
0
5
10
15
20
25
30
35
40

Fig. 42

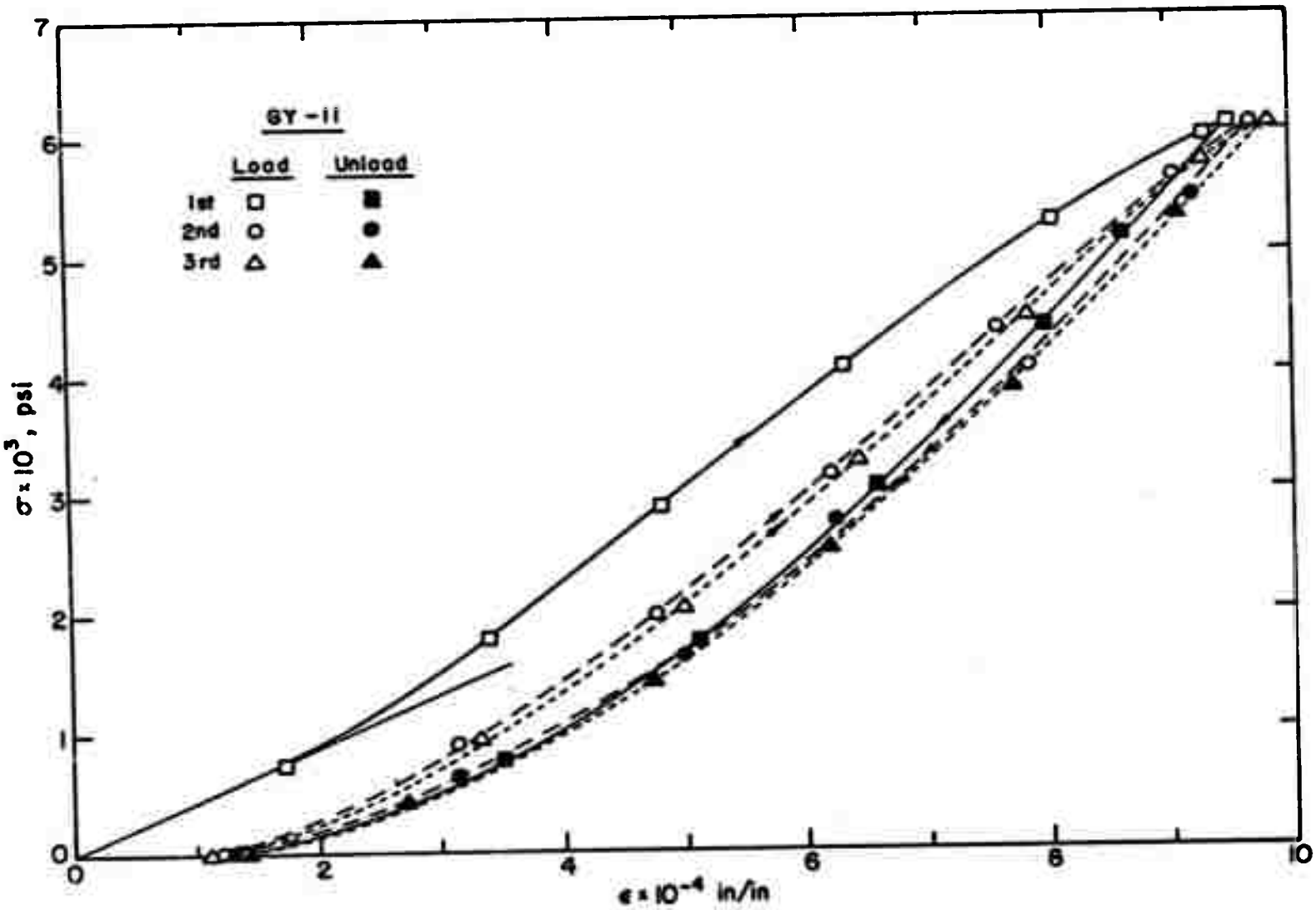
GY-11
Load
Unload
1st
2nd
3rd
σ x 10³, psi
ε x 10⁻⁴ in/in
0
1
2
3
4
5
6
7
0
2
4
6
8
10

Fig. 43

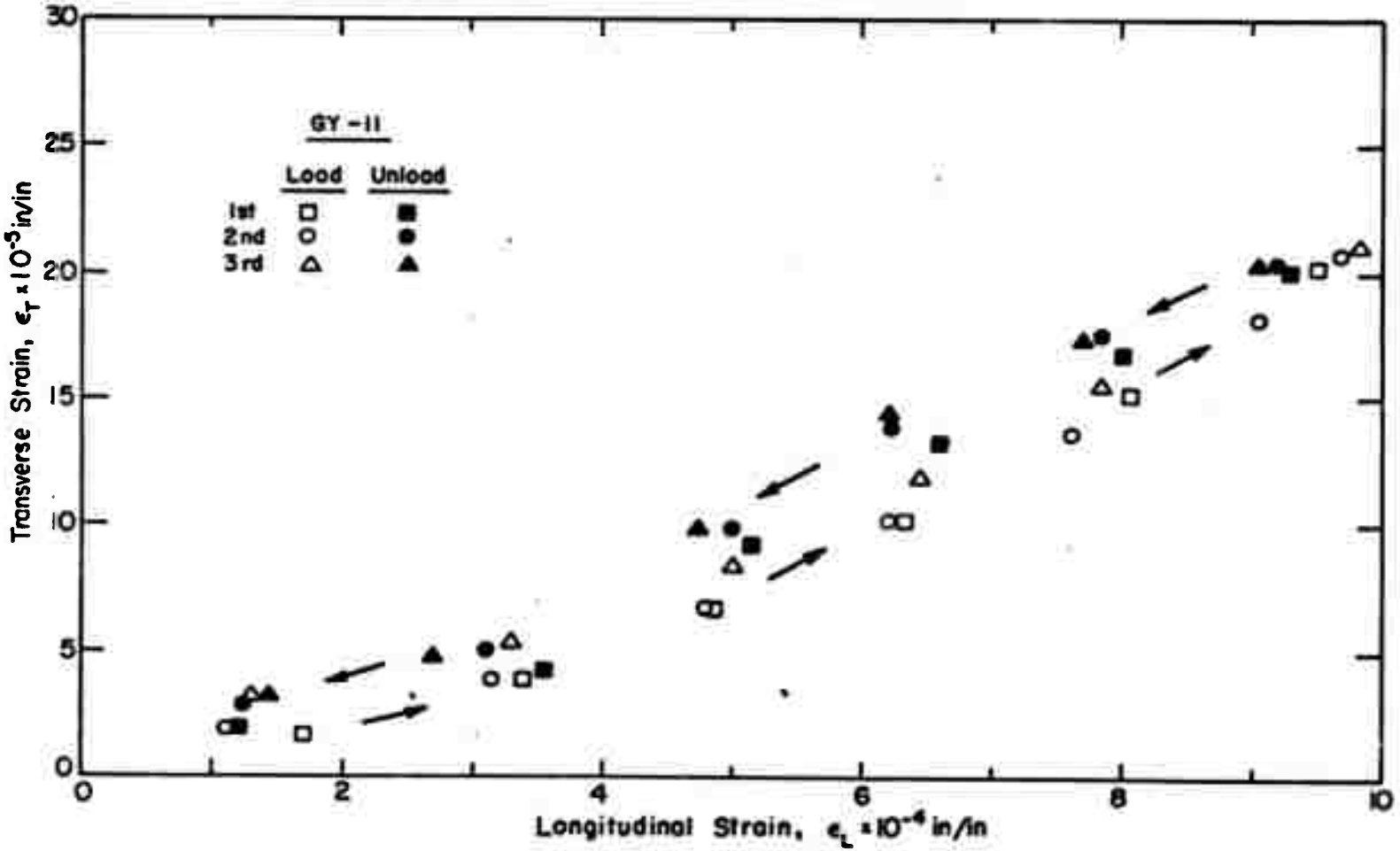
GY-11
Load
Unload
1st
2nd
3rd
Transverse Strain, $\epsilon_T \times 10^{-3}$ in/in
Longitudinal Strain, $\epsilon_L \times 10^{-4}$ in/in
0
5
10
15
20
25
30
2
4
6
8
10

Fig. 44

Fig. 45

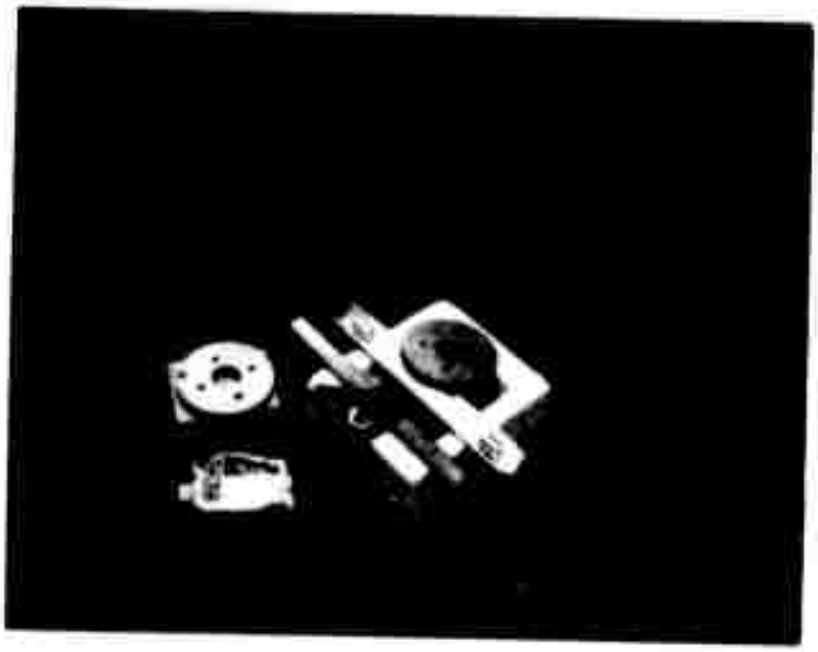

Fig. 46

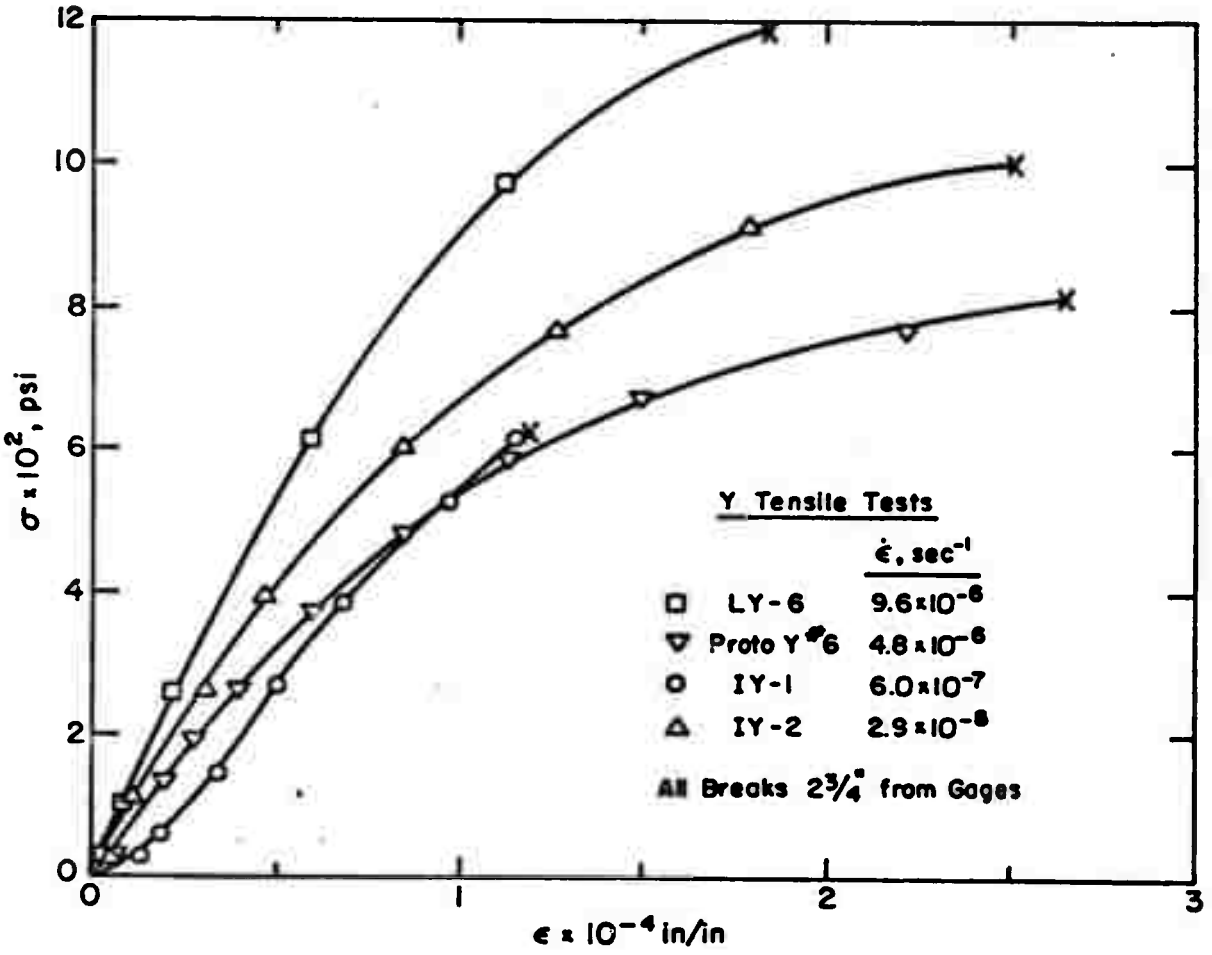
12
10
8
6
4
2
0
0
1
2
3
σ x 10², psi
ε x 10⁻⁴ in/in
Y Tensile Tests
ε̇, sec⁻¹
LY-6 9.6x10⁻⁶
Proto Y #6 4.8x10⁻⁶
IY-1 6.0x10⁻⁷
IY-2 2.9x10⁻⁸
All Breaks 2¾" from Gages

Fig. 47

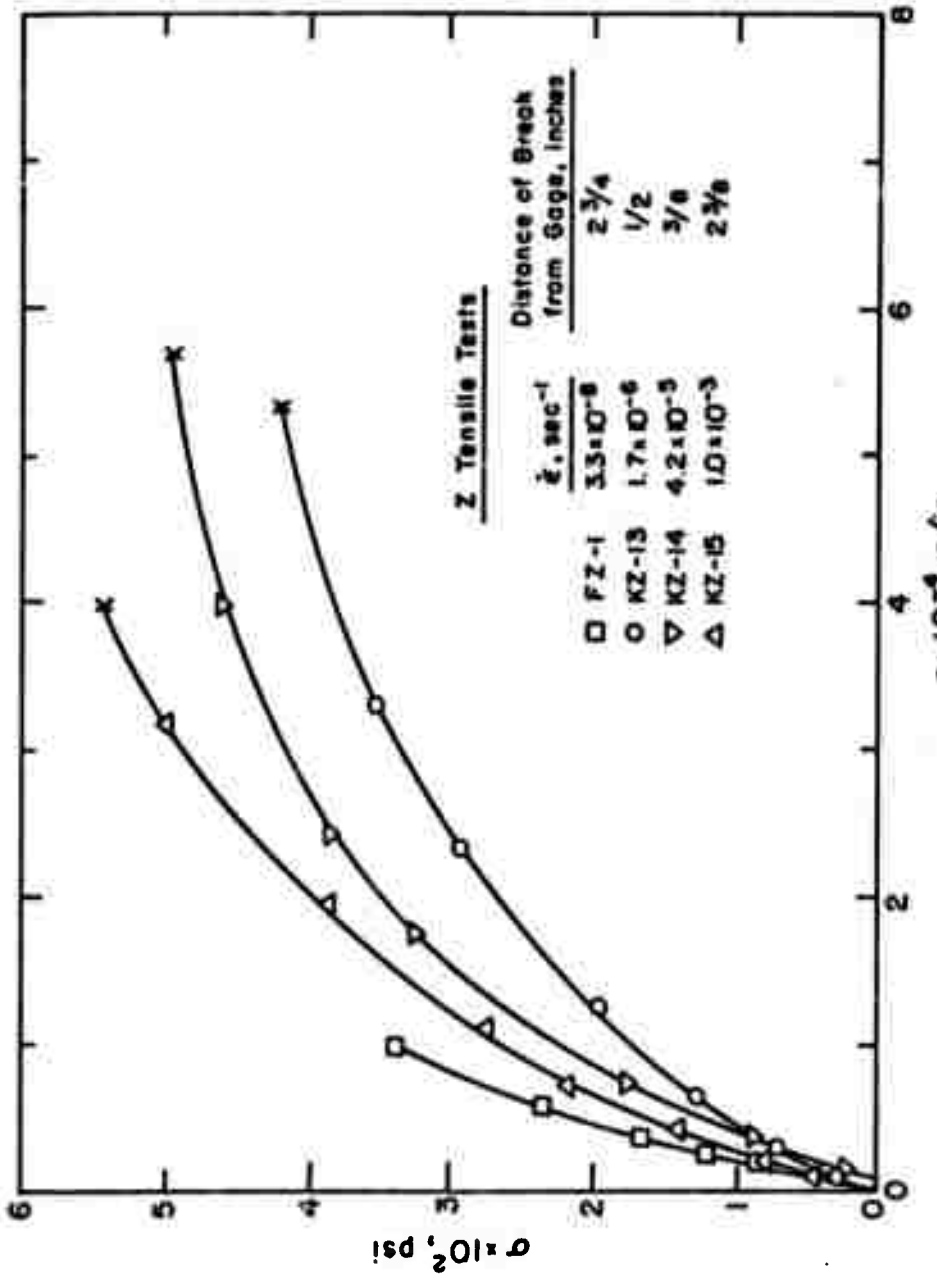
Z Tensile Tests
Distance of Break from Gage, Inches
□ FZ-1 ε̇, sec⁻¹ 3.3×10⁻⁸ 2¾
○ KZ-13 1.7×10⁻⁶ ½
▽ KZ-14 4.2×10⁻⁵ ⅜
△ KZ-15 1.0×10⁻³ 2⅜
σ ×10², psi
ε ×10⁻⁴ in/in
0
1
2
3
4
5
6
8

Fig. 48